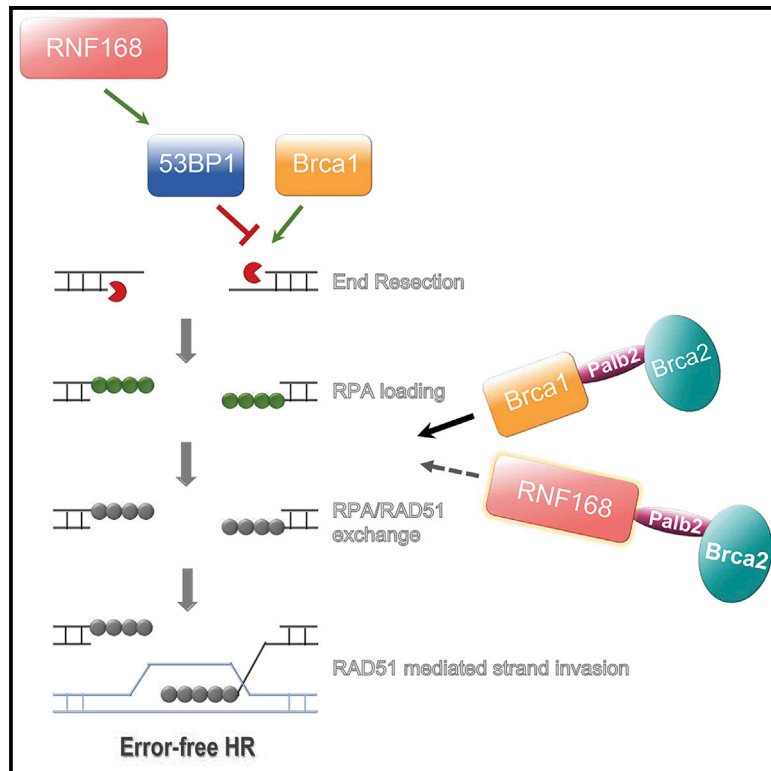Article

BRCA1 Haploinsufficiency Is Masked by RNF168-Mediated Chromatin Ubiquitylation

Graphical Abstract

Authors

Dali Zong, Salomé Adam,
Yifan Wang, ..., Neil Johnson,
Daniel Durocher, André Nussenzweig

Correspondence

andre_nussenzweig@nih.gov

In Brief

BRCA1 facilitates DNA end resection and RAD51 filament formation during homologous recombination. Zong et al. demonstrate that the RNF168-mediated chromatin ubiquitylation pathway acts redundantly with BRCA1 to promote RAD51-dependent homologous recombination. RNF168 activity is essential to prevent overt genome instability and tumorigenesis in *BRCA1* heterozygous mice, independent of *p53* mutation.

Highlights

- The E3 ubiquitin ligase RNF168 supports BRCA1-independent homologous recombination

- RNF168 acts redundantly with BRCA1 to load PALB2 onto damaged DNA

- Targeting RNF168 could induce synthetic lethality in BRCA1-deficient cancers

- The function of BRCA1 in replication fork protection is separable from its HR role

CellPress

Article

BRCA1 Haploinsufficiency Is Masked by RNF168-Mediated Chromatin Ubiquitylation

Dali Zong,[1] Salomé Adam,[2,11] Yifan Wang,[3,11] Hiroyuki Sasanuma,[4,11] Elsa Callén,[1] Matilde Murga,[5] Amanda Day,[1] Michael J. Kruhlak,[6] Nancy Wong,[1] Meagan Munro,[2] Arnab Ray Chaudhuri,[1,7] Baktiar Karim,[8] Bing Xia,[9] Shunichi Takeda,[4] Neil Johnson,[3] Daniel Durocher,[2,10] and André Nussenzweig[1,12,*]

[1]Laboratory of Genome Integrity, National Cancer Institute, NIH, Bethesda, MD, USA
[2]The Lunenfeld-Tanenbaum Research Institute, Mount Sinai Hospital, Toronto, ON, Canada
[3]Molecular Therapeutics Program, Fox Chase Cancer Center, Philadelphia, PA, USA
[4]Department of Radiation Genetics, Graduate School of Medicine, Kyoto University, Kyoto, Japan
[5]Genomic Instability Group, Spanish National Cancer Research Center, CNIO, Madrid, Spain
[6]Laboratory of Cancer Biology and Genetics, National Cancer Institute, NIH, Bethesda, MD, USA
[7]Department of Molecular Genetics, Erasmus University Medical Center, Rotterdam, the Netherlands
[8]Pathology/Histotechnology Laboratory, Frederick National Laboratory for Cancer Research, Frederick, MD, USA
[9]Department of Radiation Oncology, Rutgers Cancer Institute of New Jersey, New Brunswick, NJ, USA
[10]Department of Molecular Genetics, University of Toronto, Toronto, ON, Canada
[11]These authors contributed equally
[12]Lead Contact
*Correspondence: andre_nussenzweig@nih.gov
https://doi.org/10.1016/j.molcel.2018.12.010

SUMMARY

BRCA1 functions at two distinct steps during homologous recombination (HR). Initially, it promotes DNA end resection, and subsequently it recruits the PALB2 and BRCA2 mediator complex, which stabilizes RAD51-DNA nucleoprotein filaments. Loss of 53BP1 rescues the HR defect in BRCA1-deficient cells by increasing resection, suggesting that BRCA1's downstream role in RAD51 loading is dispensable when 53BP1 is absent. Here we show that the E3 ubiquitin ligase RNF168, in addition to its canonical role in inhibiting end resection, acts in a redundant manner with BRCA1 to load PALB2 onto damaged DNA. Loss of RNF168 negates the synthetic rescue of *BRCA1* deficiency by *53BP1* deletion, and it predisposes *BRCA1* heterozygous mice to cancer. *BRCA1*^{+/−}*RNF168*^{−/−} cells lack RAD51 foci and are hypersensitive to PARP inhibitor, whereas forced targeting of PALB2 to DNA breaks in mutant cells circumvents *BRCA1* haploinsufficiency. Inhibiting the chromatin ubiquitin pathway may, therefore, be a synthetic lethality strategy for *BRCA1*-deficient cancers.

INTRODUCTION

BRCA1 and *BRCA2* are caretaker tumor suppressors that maintain genome stability by promoting homologous recombination (HR) (Kinzler and Vogelstein, 1997). Inheritance of a single mutant allele of *BRCA1* or *BRCA2* significantly increases a person's lifetime risk for developing breast, ovarian, prostate, and other cancers (Li and Greenberg, 2012; Tutt and Ashworth, 2002). Although the tumor suppressor functions of *BRCA1* and *BRCA2* are thought to be haploinsufficient, mouse and cell line-based models of *BRCA1/2* heterozygosity do not display any measurable defects in HR (Sedic and Kuperwasser, 2016). This apparent discrepancy points to the possibility that redundancy in HR could mask latent defects in *BRCA1/2* heterozygous cells. In addition, the mechanisms for haploinsufficiency and carcinogenesis may differ between *BRCA1* and *BRCA2* heterozygous carriers. Supporting this notion, a recent study found that endogenous and environmental toxins induce haploinsufficiency in *BRCA2* mutation carriers by causing the selective proteasomal degradation of BRCA2 without affecting the level of BRCA1 protein (Tan et al., 2017). In contrast, *BRCA1*-deficient cells, but not *BRCA2*-deficient cells, are uniquely sensitive to proteasome inhibitors (Gu et al., 2014).

BRCA1 plays dual roles in HR, both by potentiating DNA end resection and by subsequently delivering RAD51 onto 3′ single-stranded DNA (ssDNA) substrates. Although its function in end resection remains unclear, BRCA1 may act in part by removing the end-blocking factor 53BP1 from chromatin surrounding DNA double-strand breaks (DSBs), which enables access and long-range resection by the DNA end-processing machinery (Bouwman et al., 2010; Bunting et al., 2010; Callen et al., 2013; Di Virgilio et al., 2013; Escribano-Díaz et al., 2013; Feng et al., 2013; Polato et al., 2014; Zimmermann et al., 2013). In addition, BRCA1 interacts with PALB2 through its coiled-coil domain, bridging it with BRCA2 post-resection, which in turn promotes the assembly of RAD51 onto 3′ ssDNA (Prakash et al., 2015). Since inactivation of *53BP1* stimulates end resection and HR proficiency in *BRCA1*-deficient cells, but not in *BRCA2*-deficient cells, it has been assumed that the loss of *53BP1* bypasses the downstream role of BRCA1 in loading RAD51. However, whereas genomic instability and embryonic lethality are rescued in *BRCA1*-deficient mouse cells (Bouwman
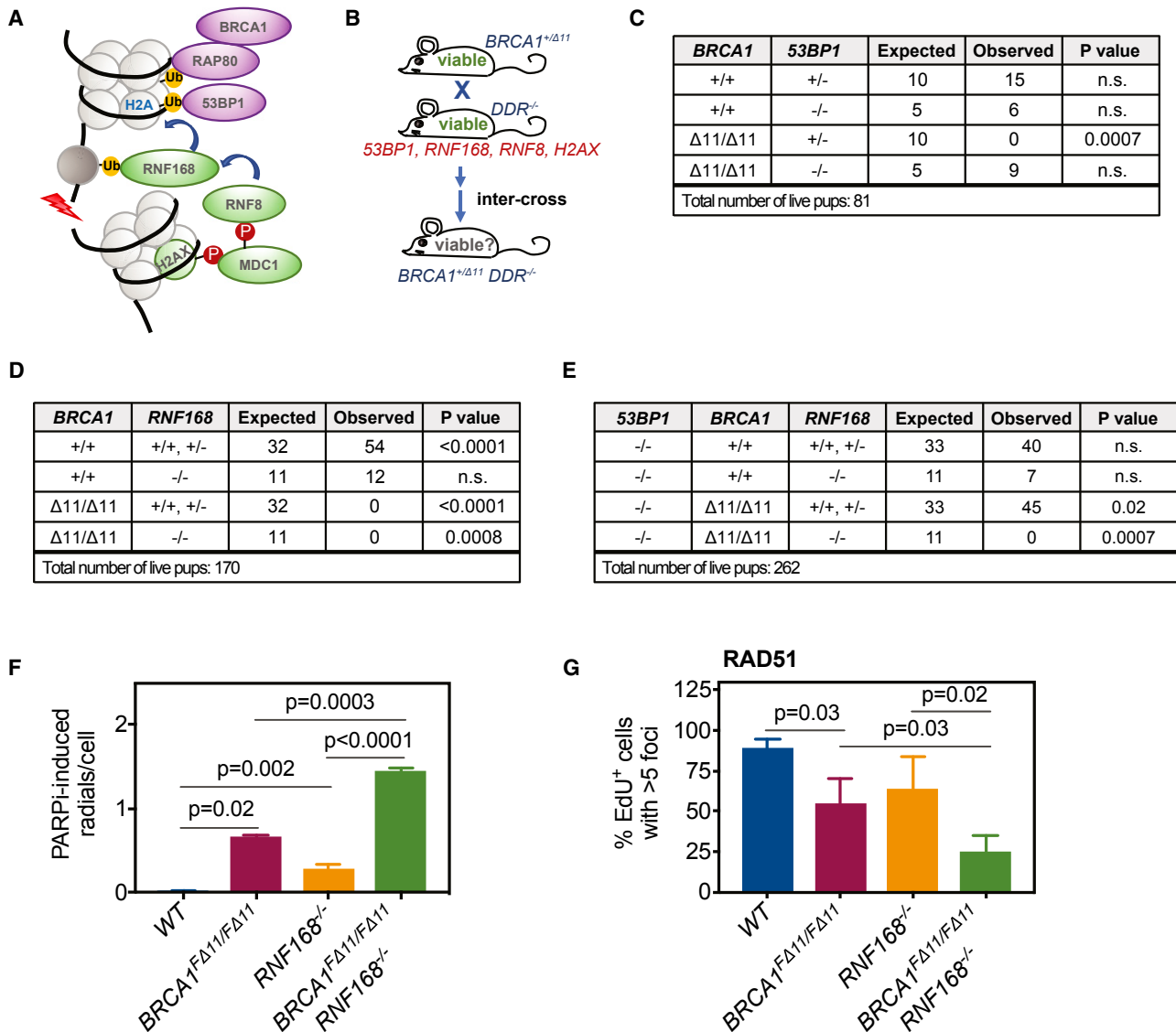
Figure 1. RNF168 Sustains Organismal Viability and Genome Maintenance When *BRCA1* Is Inactivated

(A) Model of the γ-H2AX-RNF8-RNF168 chromatin ubiquitylation pathway and downstream effectors.

(B) Breeding strategy to generate mice with combined deficiencies in *BRCA1* and the DNA damage response (DDR) factors *H2AX*, *RNF8*, *RNF168*, and *53BP1*.

(C–E) Summary of the breeding outcomes from the BRCA1$^{+/Δ11}$53BP1$^{+/-}$ × BRCA1$^{+/Δ11}$53BP1$^{-/-}$ intercross (C), the BRCA1$^{+/Δ11}$RNF168$^{+/-}$ × BRCA1$^{+/Δ11}$RNF168$^{+/-}$ intercross (D), and three intercrosses: BRCA1$^{+/Δ11}$RNF168$^{+/-}$53BP1$^{+/-}$ × BRCA1$^{+/Δ11}$RNF168$^{+/-}$53BP1$^{+/-}$, BRCA1$^{+/Δ11}$RNF168$^{+/-}$53BP1$^{-/-}$ × BRCA1$^{+/Δ11}$RNF168$^{+/-}$53BP1$^{-/-}$, and BRCA1$^{+/Δ11}$RNF168$^{+/-}$53BP1$^{-/-}$ × BRCA1$^{+/Δ11}$RNF168$^{+/-}$53BP1$^{-/-}$ (E).

(F) The average number of chromosomal radials per metaphase spread in *WT*, *BRCA1$^{FΔ11/FΔ11; CD19Cre}$*, *RNF168$^{-/-}$*, and *BRCA1$^{FΔ11/FΔ11; CD19Cre}$ RNF168$^{-/-}$* B cells exposed to PARPi.

(G) The percentage of EdU-positive (S phase) *WT*, *BRCA1$^{FΔ11/FΔ11; CD19Cre}$*, *RNF168$^{-/-}$*, and *BRCA1$^{FΔ11/FΔ11; CD19Cre}$ RNF168$^{-/-}$* B cells that stained positive for RAD51 foci 4 h post γ-irradiation (5 Gy).

Data in (F) and (G) are presented as mean ± SD. In (C)–(E) and in (F) and (G), statistical significance was calculated using the χ^2 test for goodness of fit and unpaired two-tailed Student's t test, respectively.

See also Figures S1 and S2.

et al., 2010; Bunting et al., 2010; Cao et al., 2009), the deletion of *53BP1* exacerbates genome instability in *PALB2*-knockout cells (Bowman-Colin et al., 2013), suggesting that *BRCA1*-deficient cells are capable of initiating an alternative mode of RAD51 loading when end resection is restored.

Here we demonstrate that the RNF168-mediated chromatin ubiquitylation pathway acts redundantly with BRCA1 to promote PALB2- and RAD51-dependent HR. Moreover, RNF168 activity is essential to prevent overt genome instability and tumorigenesis in *BRCA1* heterozygous mice, independent of *p53* mutation.

A TK6

B *BRCA1*$^{AID/AID}$

BRCA1$^{AID/AID}$ *53BP1*$^{-/-}$

BRCA1$^{AID/AID}$ *RNF168*$^{-/-}$, #1

BRCA1$^{AID/AID}$ *RNF168*$^{-/-}$, #2

C *BRCA1*$^{AID/AID}$ *RNF168*$^{-/-}$

D RAD51

E

F RPE1: *BRCA1*$^{-/-}$ *53BP1*$^{-/-}$

G

H

I RAD51
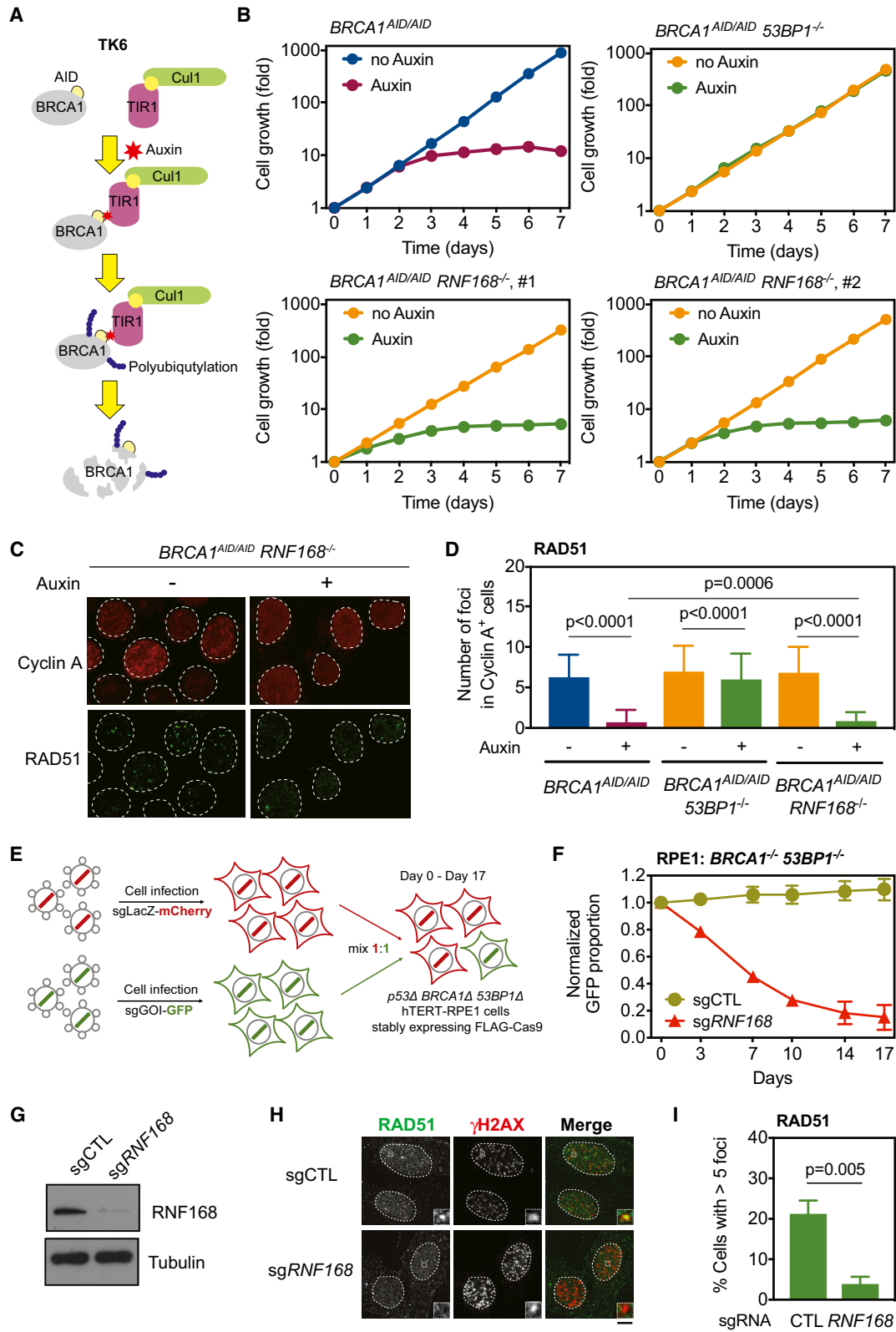
(legend on next page)

We suggest that the unmasking of *BRCA1* haploinsufficiency by RNF168 deregulation may contribute to tissue-specific cancer predisposition in *BRCA1* mutation carriers.

RESULTS

Chromatin Ubiquitylation Is Essential for HR When BRCA1 Is Inactivated

The chromatin ubiquitylation pathway, consisting of histone H2AX, MDC1, RNF8, and RNF168, regulates the retention of numerous DNA damage response (DDR) proteins, including 53BP1 and BRCA1, within a large domain flanking the actual DSB site (Figure 1A) (Altmeyer and Lukas, 2013; Messick and Greenberg, 2009; Pilch et al., 2003). In addition to its established role in promoting non-homologous end joining (NHEJ), the chromatin DDR has been implicated in HR (Adamson et al., 2012; Luijsterburg et al., 2017; Xie et al., 2004, 2007; Zhang et al., 2012). However, the physiological relevance of chromatin ubiquitylation in HR remains unknown.

To address this question, we generated a new mouse model for *RNF168* deficiency by gene targeting (Figures S1A and S1B). Like *53BP1* deficiency (Bunting et al., 2010; Manis et al., 2004; Ward et al., 2004), *RNF168* ablation led to decreased immunoglobulin class switching (Bohgaki et al., 2011) and increased ssDNA, as measured by replication protein A (RPA) foci and phosphorylation (Figures S1C–S1E), which were associated with defective 53BP1 foci formation (Figures S1F and S1G). In contrast to *53BP1*$^{-/-}$ cells (Bunting et al., 2010; Bunting and Nussenzweig, 2013), *RNF168*-deficient cells formed aberrant radial chromosomes when treated with poly(ADP-ribose) polymerase inhibitor (PARPi) or cisplatin (Figure S1H), and they exhibited a mild reduction in RAD51 foci formation (Figure S1I). Nevertheless, chromatin ubiquitylation appeared to be largely dispensable for HR in cells with unperturbed BRCA1 function.

To further determine the relationship between chromatin- and BRCA1-dependent repair, we crossed mice deficient in one allele of full-length BRCA1 (*BRCA1*$^{+/\Delta11}$) with mice lacking the chromatin DNA damage response genes *H2AX*, *RNF8*, *RNF168*, or *53BP1* (Figure 1B). As expected, homozygous *BRCA1*$^{\Delta11/\Delta11}$ deletion resulted in embryonic lethality, which was rescued by deleting *53BP1* (Figure 1C) (Bouwman et al.,

2010; Bunting et al., 2010; Cao et al., 2009). By contrast, loss of *H2AX*, *RNF8*, or *RNF168* was incompatible with viability when combined with homozygous *BRCA1*$^{\Delta11/\Delta11}$ mutation (Figures 1D, S2A, and S2B). Moreover, the loss of *RNF168* in *BRCA1*$^{\Delta11/\Delta11}$*53BP1*$^{-/-}$ mice was lethal (Figure 1E). Thus, unlike 53BP1 deficiency, abrogation of the H2AX-RNF8-RNF168 pathway does not promote BRCA1-independent survival.

The loss of *53BP1* restored genome stability in *BRCA1*$^{\Delta11/\Delta11}$ cells and largely abolished radial chromosome formation (Figure S2C) (Bouwman et al., 2010; Bunting et al., 2010). In contrast, deleting *RNF168* in conditional *BRCA1*$^{F\Delta11F/\Delta11}$ mutant B cells (i.e., CD19 CRE *BRCA1*$^{F\Delta11F/\Delta11}$*RNF168*$^{-/-}$ mice) exacerbated genome instability to levels well above those produced by each single mutant alone (Figure 1F). Moreover, RAD51 foci formation was severely compromised in the double-mutant cells (Figure 1G). Similar synergistic increases in genome instability were observed when either *H2AX* or *RNF8* was deleted in combination with *BRCA1* deficiency (Figures S2D and S2E). Altogether, these results suggest that the H2AX/RNF8/RNF168 chromatin ubiquitylation pathway becomes essential for HR when BRCA1 is functionally inactivated.

RNF168 Supports BRCA1-Independent HR in Human Cells

Despite our evidence supporting a crucial role for RNF168 in promoting BRCA1-independent HR in mice, conflicting observations have been made in human cells. Thus, small interfering RNA (siRNA) depletion of RNF168 was reported to suppress the HR defect caused by BRCA1 silencing in human cells (Muñoz et al., 2012), whereas cells co-depleted of BRCA1, 53BP1, and RNF8 showed a reduction in RAD51 foci formation (Nakada et al., 2012).

To definitively compare the impact of RNF168 versus 53BP1 loss in human cells lacking BRCA1 and avoid potential confounding factors arising from hypomorphic *BRCA1* alleles, we took advantage of an auxin-based degron system in which BRCA1 protein can be rapidly and conditionally depleted in human TK6 cells (Figures 2A and S3) (Sasanuma et al., 2018). Acute depletion of human BRCA1 resulted in a rapid cessation of proliferation followed by cell death, which was accompanied by a loss of capacity to form RAD51 foci (Figures 2B–2D). In accord

---

Figure 2. RNF168 Supports BRCA1-Independent Survival in Human Cells

(A) The auxin-induced BRCA1 degradation system in human TK6 cells.

(B) The growth profile of *BRCA1*$^{AID/AID}$, *BRCA1*$^{AID/AID}$*53BP1*$^{-/-}$, and *BRCA1*$^{AID/AID}$*RNF168*$^{-/-}$ TK6 cells in the absence and presence of 0.5 mM auxin. BRCA1 degradation induced by the addition of auxin resulted in severe growth inhibition in both *BRCA1*$^{AID/AID}$ and two independent clones of *BRCA1*$^{AID/AID}$*RNF168*$^{-/-}$ TK6 cells ($p < 0.0001$ compared to no auxin). Loss of 53BP1 rescued the growth defect in BRCA1-depleted cells.

(C) RAD51 foci formation in *BRCA1*$^{AID/AID}$, *BRCA1*$^{AID/AID}$*53BP1*$^{-/-}$, and *BRCA1*$^{AID/AID}$*RNF168*$^{-/-}$ TK6 cells 2 h post γ-irradiation (2 Gy). Cells were pre-treated or not with 0.5 mM auxin.

(D) The average number of RAD51 foci per cell among irradiated Cyclin A-positive (S/G2) TK6 cells.

(E) Outline of the Multicolor Competition Assay (MCA).

(F) MCA in *Cas9*$^+$*BRCA1*$^{-/-}$*53BP1*$^{-/-}$ human hTERT-RPE1 cells transduced with a specific guide RNA targeting *RNF168* or an empty vector (sgCTL). RPE1 cells transduced non-targeting guides (sgLacZ) were used as the competitor. Deletion of *RNF168* significantly attenuated the growth of *BRCA1*$^{-/-}$ *53BP1*$^{-/-}$ cells following PARPi treatment ($p < 0.0001$).

(G) Efficient knockdown of RNF168 in *BRCA1*$^{-/-}$*53BP1*$^{-/-}$ hTERT-RPE1 cells by CRISPR-Cas9. A representative blot is shown.

(H) RAD51 foci formation in *BRCA1*$^{-/-}$*53BP1*$^{-/-}$ hTERT-RPE1 cells transduced with either sgCTL or sg*RNF168* 4 h post γ-irradiation (5 Gy).

(I) The percentage of *BRCA1*$^{-/-}$*53BP1*$^{-/-}$ hTERT-RPE1 cells stained positive for RAD51 foci 4 h post γ-irradiation (5 Gy).

Data in (B), (D), (F), and (I) are presented as mean ± SD. In (B) and (F), in (D), and in (I), statistical significance was calculated using two-way ANOVA, Mann-Whitney test, and two-tailed Student's t test, respectively.

See also Figure S3.
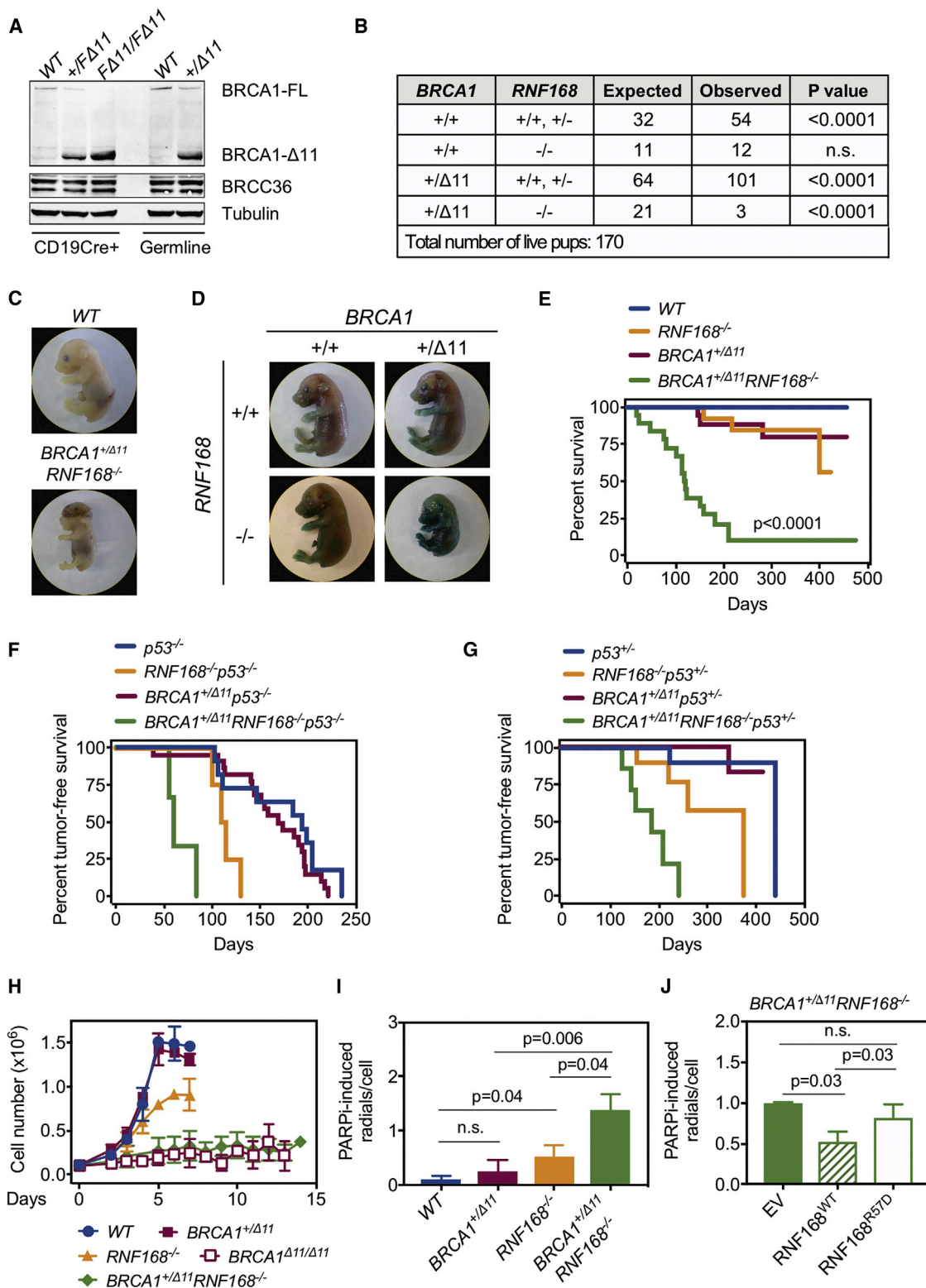
Figure 3. Loss of *RNF168* Unmasks *BRCA1* Haploinsufficiency

(A) BRCA1 protein expression level (full-length and delta-11 isoforms) in *BRCA1* heterozygous cells (*BRCA1$^{+/\Delta 11}$* and *BRCA1$^{+/F\Delta 11;\ CD19Cre}$*). *WT* and *BRCA1$^{F\Delta 11/F\Delta 11;\ CD19Cre}$* cells were used as controls.

(B) Summary of the breeding outcomes from the *BRCA1$^{+/\Delta 11}$RNF168$^{+/-}$* × *BRCA1$^{+/\Delta 11}$RNF168$^{+/-}$* intercross.

(legend continued on next page)

with mouse studies (Bouwman et al., 2010; Bunting et al., 2010), deletion of *53BP1* by CRISPR-Cas9 rescued these phenotypes (Figures 2B and 2D). In contrast, deletion of *RNF168* failed to restore the growth defect in BRCA1-depleted cells (Figure 2B). Moreover, RNF168 deficiency did not rescue RAD51 foci formation in BRCA1-depleted human TK6 cells (Figures 2C and 2D). Consistent with the observation in TK6, single-guide RNA (sgRNA) targeting *RNF168* was able to reverse the PARPi-resistant phenotype of human RPE1 cells in which both *BRCA1* and *53BP1* had been deleted using CRISPR-Cas9 (Figures 2E and 2F). Finally, the loss of RNF168 significantly impaired damage-induced RAD51 foci formation in *BRCA1*−/−*53BP1*−/− RPE1 cells (Figures 2G–2I). Thus, RNF168 is required to support BRCA1-independent survival and RAD51 foci formation in both mouse and human cells.

RNF168 Deletion Reveals BRCA1 Haploinsufficiency

Although mutation of a single *BRCA1* allele leads to cancer predisposition, mouse models of *BRCA1* heterozygosity do not show genome instability or tumorigenesis (Berton et al., 2003; Sedic and Kuperwasser, 2016; Xu et al., 2001). Given the severe impact of RNF168 loss in *BRCA1*$^{\Delta11/\Delta11}$ cells (Figures 1F and 1G), we wished to determine whether RNF168 activity might also be essential in *BRCA1* heterozygous cells. We first verified that cells derived from *BRCA1*$^{+/\Delta11}$ and *BRCA1*$^{+/F\Delta11}$ heterozygous mice expressed full-length BRCA1 at approximately 50% the level detected in wild-type (WT) controls (Figure 3A). As expected, *BRCA1*$^{+/\Delta11}$ heterozygous mice expressing RNF168 were born at normal frequency and did not exhibit any notable phenotypes. However, deletion of *RNF168* had a profound impact on the viability of heterozygous *BRCA1*$^{+/\Delta11}$ mice. Live *BRCA1*$^{+/\Delta11}$*RNF168*−/− pups were born at significantly sub-Mendelian frequencies, even though both *BRCA1*$^{+/\Delta11}$ and *RNF168*−/− mice were born at normal frequencies (Figure 3B). While *BRCA1*$^{+/\Delta11}$*RNF168*−/− embryos were observed on embryonic day (E)16.5 (Figures S4A and S4B), these embryos showed severe growth retardation and stained positive for senescence-associated β-galactosidase, indicative of senescence (Figures 3C, 3D, S4C, and S4D). Moreover, a substantial fraction of *BRCA1*$^{+/\Delta11}$*RNF168*−/− embryos exhibited additional gross developmental abnormalities, including exencephaly, mi-

crophthalmia, and anophthalmia (Figures 3C, S4C, and S4D). We conclude that *RNF168* loss reveals latent defects associated with *BRCA1* heterozygosity.

Despite the fact that *BRCA1*$^{+/\Delta11}$*RNF168*−/− pups were born at sub-Mendelian frequencies, we eventually obtained a cohort of live pups through extensive breeding (19 of 68 expected, total n = 727, p < 0.0001), but they were consistently smaller than their *BRCA1*$^{+/\Delta11}$ littermates (Figure S4E). *BRCA1*$^{+/\Delta11}$*RNF168*−/− mice exhibited significantly shortened lifespan with a median survival of 120 days, as compared to either *BRCA1*$^{+/\Delta11}$ or *RNF168*−/− single-mutant littermates (343 and 372 days, respectively) (Figure 3E). Moreover, 9 of 19 *BRCA1*$^{+/\Delta11}$*RNF168*−/− mice spontaneously developed lymphoma (Figure S4F), and the loss of RNF168 also accelerated tumorigenesis in both *BRCA1*$^{+/\Delta11}$*p53*−/− and *BRCA1*$^{+/\Delta11}$*p53*+/− mice (Figures 3F and 3G). Thus, while *p53* deficiency alone does not foster *BRCA1* haploinsufficiency for tumor formation (Berton et al., 2003; Sedic and Kuperwasser, 2016; Xu et al., 2001), *BRCA1* heterozygous mice become tumor prone when RNF168 is lost.

The loss of BRCA1 causes a rapid onset of senescence in cultured cells (Cao et al., 2009). Similarly, we found that primary mouse embryonic fibroblasts (MEFs) derived from E13.5 *BRCA1*$^{+/\Delta11}$*RNF168*−/− embryos grew poorly and senesced prematurely (Figure 3H). By contrast, heterozygous *BRCA1*$^{+/\Delta11}$ cells grew normally in culture, while *RNF168*−/− cells exhibited a relatively mild growth delay (Figure 3H). Moreover, *BRCA1*$^{+/\Delta11}$*RNF168*−/− MEFs and splenic B cells exhibited high levels of genome instability when exposed to PARPi or cisplatin (Figures 3I, S5A, and S5B), in a manner dependent on H2A-K13/K15 ubiquitylation, as inferred using the separation-of-function RNF168^{R57D} mutant (Mattiroli et al., 2012) (Figure 3J). Finally, *BRCA1*$^{+/\Delta11}$*RNF168*−/− cells exhibited reduced short-term viability and clonogenic survival upon treatment with PARPi and cisplatin (Figures S5C–S5F). Together, these data demonstrate that BRCA1 becomes haploinsufficient for genome maintenance in the absence of H2A-directed RNF168 ubiquitin ligase activity.

BRCA1-Independent PALB2 Loading Requires RNF168

It was recently demonstrated that RNF168 promotes an alternative mode of recruitment of PALB2 to damaged chromatin (Luijsterburg et al., 2017). Since RNF168 is dispensable for RAD51

(C) Representative morphology of E16.5 *WT* and *BRCA1*$^{+/\Delta11}$*RNF168*−/− embryos. The latter exhibited growth retardation as well as exencephaly.

(D) Staining of E16.5 embryos for senescence-associated β-galactosidase activity.

(E) Kaplan-Meier survival analysis of *WT* (n = 8), *BRCA1*$^{+/\Delta11}$ (n = 16), *RNF168*−/− (n = 13), and *BRCA1*$^{+/\Delta11}$*RNF168*−/− (n = 19) mice. A significantly shorter lifespan was observed in *BRCA1*$^{+/\Delta11}$*RNF168*−/− mice compared to the *RNF168*−/− counterparts (p < 0.0001).

(F) Kaplan-Meier survival analysis of *p53*−/− (n = 11), *BRCA1*$^{+/\Delta11}$*p53*−/− (n = 22), *RNF168*−/−*p53*−/− (n = 4), and *BRCA1*$^{+/\Delta11}$*RNF168*−/−*p53*−/− (n = 3) mice. A significantly shorter tumor-free survival was observed in *BRCA1*$^{+/\Delta11}$*RNF168*−/−*p53*−/− mice compared to *BRCA1*$^{+/\Delta11}$*p53*−/− and *RNF168*−/−*p53*−/− counterparts (p < 0.0001 and p = 0.01, respectively).

(G) Kaplan-Meier survival analysis of *p53*+/− (n = 10), *BRCA1*$^{+/\Delta11}$*p53*+/− (n = 11), *RNF168*−/−*p53*+/− (n = 10), and *BRCA1*$^{+/\Delta11}$*RNF168*−/−*p53*+/− (n = 8) mice. A significantly shorter tumor-free survival was observed in *BRCA1*$^{+/\Delta11}$*RNF168*−/−*p53*+/− mice compared to *BRCA1*$^{+/\Delta11}$*p53*−/− and *RNF168*−/−*p53*−/− counterparts (p < 0.0001 and p = 0.003, respectively).

(H) Growth of *WT*, *BRCA1*$^{+/\Delta11}$, *RNF168*−/−, and *BRCA1*$^{+/\Delta11}$*RNF168*−/− primary mouse embryonic fibroblasts (MEFs) in culture. *BRCA1*$^{+/\Delta11}$*RNF168*−/− cells grew significantly slower than *BRCA1*$^{+/\Delta11}$ and *RNF168*−/− counterparts (p = 0.02, Kruskal-Wallis test).

(I) The average number of chromosomal radials per metaphase spread in *WT*, *BRCA1*$^{+/\Delta11}$, *RNF168*−/−, and *BRCA1*$^{+/\Delta11}$*RNF168*−/− MEFs exposed to PARPi.

(J) The average number of chromosomal radials per metaphase spread in PARPi-treated *BRCA1*$^{+/\Delta11}$*RNF168*−/− MEFs stably expressing WT or catalytic mutant (R57D) forms of RNF168. *BRCA1*$^{+/\Delta11}$*RNF168*−/− MEFs transduced with empty vector (EV) were used as the control.

Data in (G)–(I) are presented as mean ± SD. In (B) and in (H), statistical significance was calculated using the χ^2 test for goodness of fit and one-way ANOVA, respectively. In (E)–(G) and in (I) and (J), statistical significance was calculated using the Mantel-Cox test and unpaired two-tailed Student's t test, respectively. See also Figures S4 and S5.
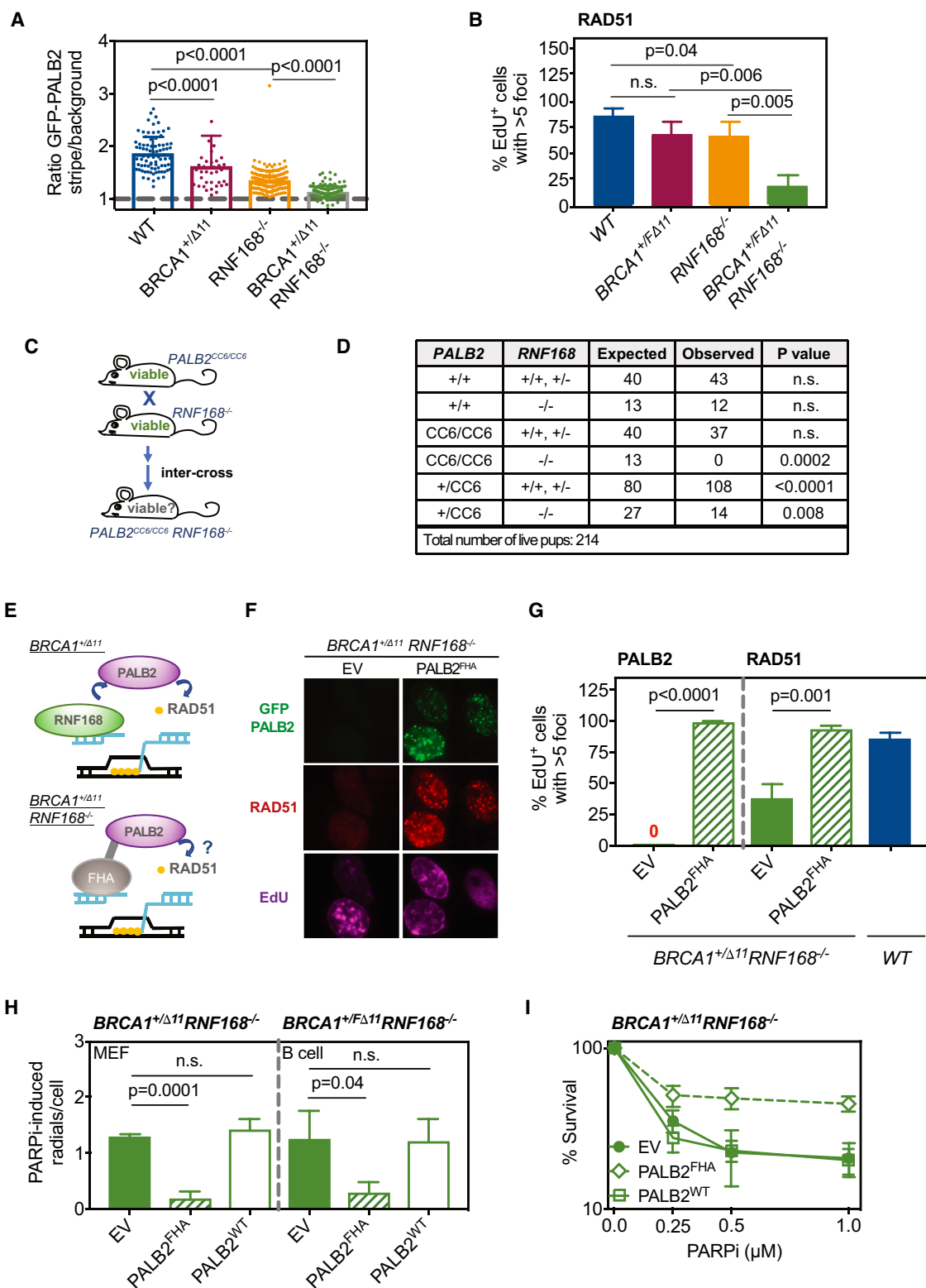
Figure 4. RNF168-Mediated PALB2 Recruitment Is Essential for Viability and Genome Maintenance When the BRCA1-PALB2 Pathway Is Compromised

(A) The average fluorescence intensity of PALB2 stripes in *WT*, *BRCA1$^{+/\Delta11}$*, *RNF168$^{-/-}$*, and *BRCA1$^{+/\Delta11}$RNF168$^{-/-}$* MEFs stably expressing GFP-PALB2. Signals were normalized to the background noise.

(legend continued on next page)

foci (Figure S1I) and organismal viability whereas PALB2 is essential (Bowman-Colin et al., 2013; Rantakari et al., 2010), absence of the chromatin ubiquitin pathway alone should not abrogate HR *in vivo*. In agreement with Luijsterburg et al. (2017), we found that the H2A ubiquitylation activity of RNF168, but not 53BP1, promoted the formation of irradiation-induced PALB2 foci (Figures S6A and S6B). Since BRCA1 is a major facilitator of PALB2 recruitment (Sy et al., 2009; Zhang et al., 2009a, 2009b), we hypothesized that RNF168-deficient cells might still be able to recruit PALB2 to DNA-damaged sites, insufficient to be observed as distinct foci but ample enough to load RAD51.

To examine DSB recruitment independent of large-scale focal accumulation (Bekker-Jensen et al., 2006; Celeste et al., 2003), we subjected cells to laser micro-irradiation, and we measured the accumulation of PALB2 along the damaged tracks marked by γ-H2AX. Compared to WT cells, $BRCA1^{+/\Delta11}$ cells and $RNF168^{-/-}$ cells exhibited a reduction in PALB2 accumulation at damage sites, but PALB2 recruitment was barely detectable in $BRCA1^{+/\Delta11}RNF168^{-/-}$ cells (Figure 4A). Moreover, while $RNF168^{-/-}$ and $BRCA1^{+/\Delta11}$ cells were largely competent for RAD51 foci formation (Figures S1I and S6C), there was a severe defect in RAD51 loading in $BRCA1^{+/\Delta11}RNF168^{-/-}$ cells (Figure 4B), which correlated with the synergistic increase in genome instability (Figures 3I, S5A, and S5B). Thus, BRCA1 and RNF168 act cooperatively to facilitate RAD51 assembly and maintain genome stability.

In contrast to the severe impact of RNF168 loss in *BRCA1*-deficient cells, loss of RNF168 in *BRCA2*-deficient cells did not further enhance genome instability (Figure S6D). These data suggest that BRCA1-independent RAD51 loading via PALB2/BRCA2 requires RNF168. Consistent with this, inactivation of *PALB2* or *BRCA2* by CRISPR-Cas9 re-sensitized $BRCA1^{-/-}53BP1^{-/-}$ human RPE1 cells to PARPi (Figure S6E), similar to *RNF168* deletion (Figure 2F). Thus, *BRCA1* heterozygous cells and $BRCA1^{-/-}53BP1^{-/-}$ cells rely on RNF168 to sustain a critical level of PALB2 recruitment that is sufficient for RAD51-dependent HR and normal growth.

To determine whether RNF168-mediated PALB2 recruitment is separable from the canonical BRCA1-dependent PALB2 response, we took advantage of a recent mouse model in which mutations have been introduced into the PALB2 coiled-coil domain to produce a mutant PALB2 protein ($PALB2^{CC6}$) that is unable to interact with BRCA1 (Figure 4C) (Simhadri et al., 2014). Unlike mice with a complete knockout of *PALB2* or *BRCA1*, $PALB2^{CC6/CC6}$ mice are viable, suggesting another loading platform for PALB2 could substitute for BRCA1 (Simhadri et al., 2014). Similar to *BRCA1/RNF168* deficiency, combining $PALB2^{CC6/CC6}$ homozygosity with *RNF168* deficiency was incompatible with viability, and $PALB2^{CC6/CC6}RNF168^{-/-}$ embryos died before E16.5 (Figures 4D and S6F). Moreover, partial loss of the PALB2/BRCA1 interaction in $PALB2^{+/CC6}RNF168^{-/-}$ cells led to increased PARPi- and cisplatin-induced genomic instability relative to $PALB2^{+/CC6}$, $RNF168^{-/-}$, or even $PALB2^{CC6/CC6}$ cells (Figures S6G and S6H). Thus, when either BRCA1 levels or its interaction with PALB2 is decreased by 50%, cells rely on the RNF168-dependent mode of PALB2 recruitment to sustain HR.

Forced Loading of PALB2 to Chromatin Bypasses BRCA1 Haploinsufficiency

Based on the observation that RNF168 ubiquitin ligase activity is critical for genome integrity in $BRCA1^{+/\Delta11}$ cells, we hypothesized that the requirement for RNF168 activity in $BRCA1^{+/\Delta11}$ cells might be circumvented if PALB2 could be forced to accumulate at DNA breaks. To accomplish this, we fused the Forkhead associated domain (FHA) domain of RNF8, which recognizes phosphorylated MDC1 at sites of DNA damage (Huen et al., 2007; Kolas et al., 2007; Mailand et al., 2007), in frame to PALB2 (Figure 4E). The resultant fusion protein, $PALB2^{FHA}$, was able to form foci in response to DNA damage in cells lacking RNF168 (Figures 4F and 4G). $PALB2^{FHA}$ also restored RAD51 foci formation in $BRCA1^{+/\Delta11}RNF168^{-/-}$ cells to levels comparable to those found in WT controls (Figures 4F and 4G). Moreover, $PALB2^{FHA}$ expression reduced the formation of toxic chromosomal radials in $BRCA1^{+/\Delta11}RNF168^{-/-}$ cells (Figure 4H), and it alleviated their hypersensitivity to PARPi (Figure 4I). Thus, the requirement of RNF168 for genome maintenance in *BRCA1* heterozygous cells can be bypassed by augmenting PALB2 binding to damaged chromatin.

Chromatin Ubiquitylation Is Dispensable in BRCA1 Mutants that Retain Interaction with PALB2

The risk of carcinogenesis among mutation carriers is dependent on the nature of the germline *BRCA1* mutation (Wang et al.,

(B) The percentage of EdU-positive (S phase) *WT*, $BRCA1^{+/F\Delta11; CD19Cre}$, $RNF168^{-/-}$, and $BRCA1^{+/F\Delta11; CD19Cre} RNF168^{-/-}$ B cells that stained positive for RAD51 foci 4 h post γ-irradiation (5 Gy).

(C) Breeding strategy for the generation of mice lacking *RNF168* in the context of an abrogated BRCA1-PALB2 interaction ($PALB2^{CC6}$).

(D) Summary of the breeding outcomes from the $PALB2^{+/CC6}RNF168^{+/-} \times PALB2^{+/CC6}RNF168^{+/-}$ intercross.

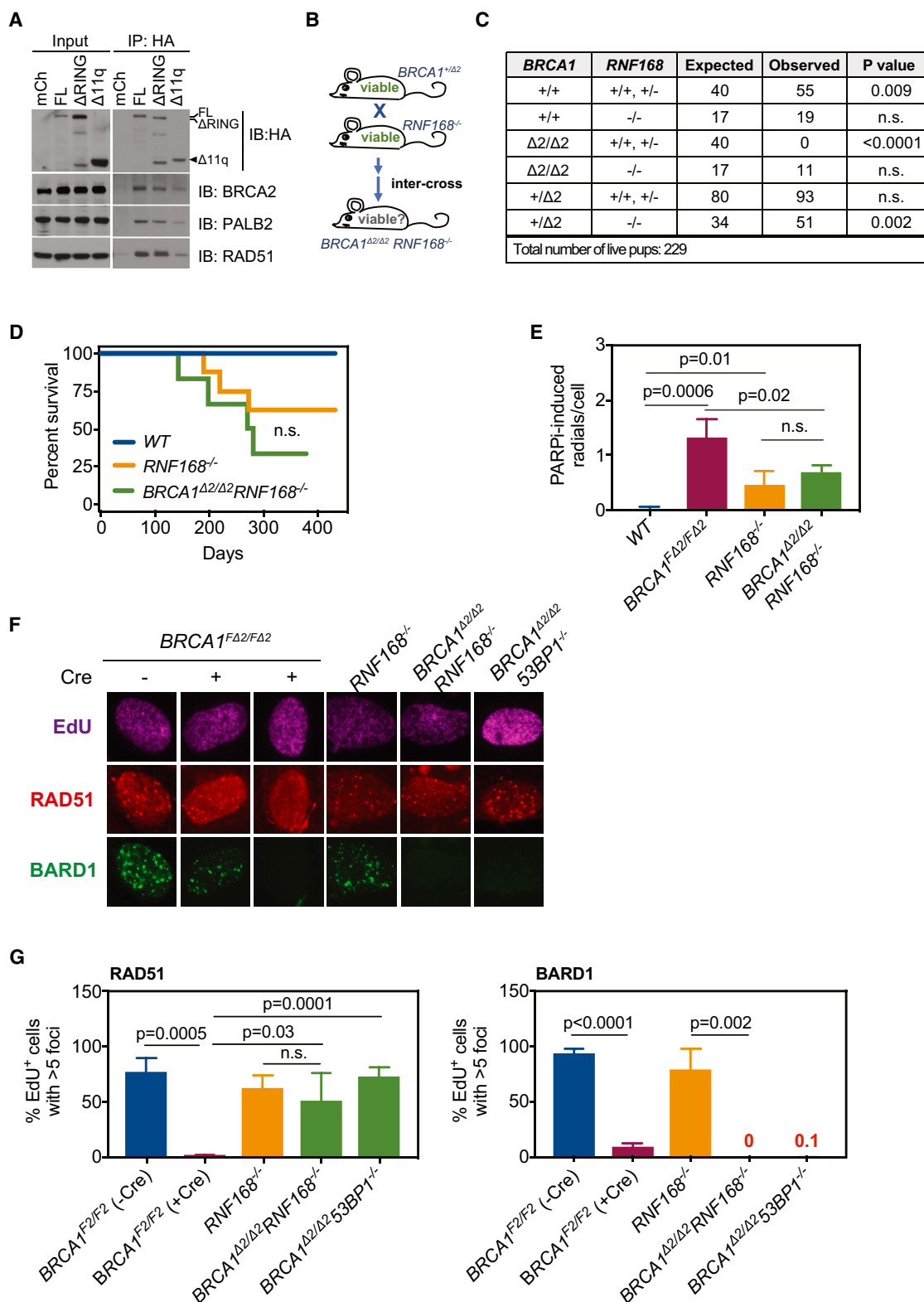(E) Strategy for forced targeting of PALB2 to DSB sites.

(F) Formation of PALB2 and RAD51 foci in $BRCA1^{+/\Delta11}RNF168^{-/-}$ MEFs stably expressing GFP-PALB2^{FHA}.

(G) The percentage of EdU-positive (S phase) $BRCA1^{+/\Delta11}RNF168^{-/-}$ MEFs stably expressing GFP-PALB2^{FHA} that stained positive for PALB2 and RAD51 foci 4 h post γ-irradiation (10 Gy). *WT* MEFs and $BRCA1^{+/\Delta11}RNF168^{-/-}$ MEFs transduced with empty vector (EV) were used as controls.

(H) The average number of chromosomal radials per metaphase spread in PARPi-treated $BRCA1^{+/\Delta11}RNF168^{-/-}$ MEFs and $BRCA1^{+/F\Delta11; CD19Cre} RNF168^{-/-}$ B cells stably expressing WT PALB2 or PALB2^{FHA}.

(I) Colony formation capacity of $BRCA1^{+/\Delta11}RNF168^{-/-}$ MEFs stably expressing WT PALB2 or PALB2^{FHA} after treatment with PARPi. PALB2^{FHA} expression significantly rescued PARPi hypersensitivity in $BRCA1^{+/\Delta11}RNF168^{-/-}$ MEFs (p < 0.0001). In (H) and (I), MEFs and B cells transduced with empty vector (EV) were used as controls.

Data in (A), (B), and (G)–(I) are presented as mean ± SD. In (A) and (D), statistical significance was calculated using the Mann-Whitney test and χ^2 test for goodness of fit, respectively. In (G) and (H) and in (I), statistical significance was calculated using unpaired two-tailed Student's t test and two-way ANOVA, respectively. See also Figure S6.

Figure 5. RNF168 Function Is Dispensable in a BRCA1 Mutant that Retains Interaction with PALB2

(A) Co-immunoprecipitation of BRCA1-interacting proteins in BRCA1-null human MDA-MB-436 cells stably expressing full-length (FL), ΔRING, and Δ11q iso-forms of BRCA1. Cells expressing empty vector (mCherry) were used as the control.

2016a). A mutant form of BRCA1 lacking exon 11 (BRCA1-Δ11q) was found to be expressed in human breast cancer cells, and it showed reduced efficiency of interaction with PALB2 compared to full-length BRCA1 (Wang et al., 2016a) (Figure 5A). As BRCA1-Δ11q is nearly identical to the mouse BRCA1-Δ11 protein, we hypothesized that this explains why mutant $BRCA1^{+/\Delta11}$, $BRCA1^{\Delta11/\Delta11}$, and $BRCA1^{\Delta11/\Delta11}53BP1^{-/-}$ cells become reliant on RNF168 for loading RAD51. Indeed, even $BRCA1^{+/\Delta11}$ cells showed a reduction in PALB2 accumulation at damage sites (Figure 4A). By contrast, a mutant form of BRCA1 lacking the N-terminal RING domain (BRCA1-ΔRING) (Drost et al., 2016; Wang et al., 2016b) was able to maintain interaction with PALB2, BRCA2, and RAD51, similar to full-length BRCA1 (Figure 5A).

Mice carrying homozygous deletion of *BRCA1* exon 2 produce a mutant RING-less BRCA1 protein (BRCA1-Δ2) that is structurally similar to human BRCA1-ΔRING (Li et al., 2016). Since BRCA1-Δ2 maintains an intact PALB2 interaction domain (Drost et al., 2016; Li et al., 2016; Wang et al., 2016b), we speculated that $BRCA1^{\Delta2/\Delta2}$ mice would not be reliant on an RNF168-dependent pathway for loading PALB2 (Figure 5B). Consistent with this, and contrary to the synthetic lethality imparted on $BRCA1^{\Delta11/\Delta11}$ and $BRCA1^{+/\Delta11}$ mice, RNF168 deficiency rescued the early embryonic lethality in $BRCA1^{\Delta2/\Delta2}$ mice (Ludwig et al., 1997) (Figure 5C). $BRCA1^{\Delta2/\Delta2} RNF168^{-/-}$ mice survived at least 143 days (median survival 275 days), similar to mice lacking only *RNF168* (median survival 281 days), and they were not more tumor prone than the latter (Figure 5D). On the contrary, $BRCA1^{+/\Delta11} RNF168^{-/-}$ mice had a shorter median survival (120 days) and developed tumors at a younger age (Figure 3E; Figure S4F). $BRCA1^{\Delta2/\Delta2} RNF168^{-/-}$ cells exhibited only slightly higher levels of PARPi-induced radial chromosomes to those observed in $RNF168^{-/-}$ cells (Figure 5E). Moreover, while RAD51 foci formation was severely compromised in conditionally deleted $BRCA1^{F\Delta2/F\Delta2}$ MEFs (marked by the loss of BARD1 protein), RAD51 foci were largely restored in $BRCA1^{\Delta2/\Delta2} RNF168^{-/-}$ MEFs derived from compound homozygous mutant mice (Figures 5F and 5G). These data are consistent with the idea that increased resection alone can circumvent the HR defects in *BRCA1* mutants that maintain their interaction with PALB2. However, rescuing *BRCA1* mutants with impaired BRCA1-PALB2 interaction requires both increased resection and RNF168-dependent PALB2 loading.

RNF168 Does Not Cooperate with BRCA1 in Replication Fork Protection

Recent studies suggest that replication stress response pathways may be partially defective in cells from heterozygous *BRCA1* and *PALB2* mutation carriers (Nikkilä et al., 2013; Pathania et al., 2014). Moreover, the inability to protect stalled replication forks contributes to DNA damage-induced cytotoxicity (Ray Chaudhuri et al., 2016). This raises the possibility that PARPi and cisplatin hypersensitivity evident in $BRCA1^{+/\Delta11}RNF168^{-/-}$ cells could result from defects in replication fork protection as well as HR. However, loss of *RNF168* did not further increase nucleolytic degradation of replication forks, regardless of *BRCA1* mutation ($BRCA1^{+/\Delta11}$ or $BRCA1^{\Delta2/\Delta2}$) (Figures 6A and 6B). Interestingly, the BRCA1 RING domain, though essential for HR, was dispensable for replication fork protection, whereas *BRCA1* exon 11 is essential for both (Ray Chaudhuri et al., 2016). We conclude that the impairment of RAD51-dependent HR, but not replication fork protection, underlies the synthetic lethal interaction between $BRCA1^{+/\Delta11}$ and *RNF168*.

DISCUSSION

The γ-H2AX-RNF8-RNF168 ubiquitin cascade triggers DNA repair factor recruitment to chromatin flanking DSBs through sequential ubiquitylation of histones H1 and H2A (Doil et al., 2009; Stewart et al., 2009; Stucki et al., 2005; Thorslund et al., 2015; Wilson et al., 2016). Chromatin ubiquitylation is required for the concentration and spreading of DNA damage response proteins distal to the actual break site, but it is dispensable for proximal break site recruitment (Bekker-Jensen et al., 2006; Celeste et al., 2003). The precise function of chromatin ubiquitylation surrounding break sites remains unclear, as deficiency in H2AX/RNF8/RNF168 impairs a subset of chromatin-related DSB repair and signaling functions, none of which is essential for viability (Bohgaki et al., 2011; Celeste et al., 2002; Santos et al., 2010).

Our results indicate that, in addition to opposing the initial resection step of HR, the ubiquitin pathway acts as a backup to BRCA1 at a later step of HR that connects it with PALB2 and RAD51 (Figure 6C). Similar to BRCA1 (Bekker-Jensen et al., 2006; Coleman and Greenberg, 2011; Hu et al., 2011; Messick and Greenberg, 2009), PALB2 appears to engage both the flanking chromatin and the ssDNA compartments proximal to

(B) Breeding strategy for the generation of mice lacking *RNF168* in the context of homozygous $BRCA1^{\Delta2/\Delta2}$ mutation.

(C) Summary of the breeding outcomes from two intercrosses: $BRCA1^{+/\Delta2}RNF168^{+/-}$ × $BRCA1^{+/\Delta2}RNF168^{+/-}$ and $BRCA1^{+/\Delta2}RNF168^{+/-}$ × $BRCA1^{+/\Delta2}RNF168^{-/-}$.

(D) Kaplan-Meier survival analysis of *WT* (n = 6), $RNF168^{-/-}$ (n = 9), and $BRCA1^{\Delta2/\Delta2}RNF168^{-/-}$ (n = 6) mice. Overall survival was comparable between $BRCA1^{\Delta2/\Delta2}RNF168^{-/-}$ and $RNF168^{-/-}$ mice (p = 0.31).

(E) The average number of chromosomal radials per metaphase spread in *WT*, $BRCA1^{F\Delta2/F\Delta2; CD19Cre}$, $RNF168^{-/-}$, and $BRCA1^{\Delta2/\Delta2} RNF168^{-/-}$ B cells exposed to PARPi.

(F) RAD51 and BARD1 foci formation in *WT* ($BRCA1^{F\Delta2/F\Delta2}$ no Cre), $BRCA1^{\Delta2/\Delta2}$ ($BRCA1^{F\Delta2/F\Delta2}$ + Ad-Cre), $RNF168^{-/-}$, and $BRCA1^{\Delta2/\Delta2} RNF168^{-/-}$ MEFs 4 h post γ-irradiation (5 Gy). Note that a small fraction (<10%) of $BRCA1^{F\Delta2/F\Delta2}$ + AdCre MEFs retain robust BARD1 foci formation under these conditions. The majority of such cells also stain positive for RAD51 foci.

(G) The percentage of EdU-positive (S phase) *WT* ($BRCA1^{F\Delta2/F\Delta2}$ no Cre), $BRCA1^{\Delta2/\Delta2}$ ($BRCA1^{F\Delta2/F\Delta2}$ + Ad-Cre), $RNF168^{-/-}$, and $BRCA1^{\Delta2/\Delta2} RNF168^{-/-}$ MEFs that stained positive for RAD51 (left panel) or BARD1 (right panel) foci 4 h post γ-irradiation (5 Gy). For $BRCA1^{F\Delta2/F\Delta2}$ + AdCre MEFs, RAD51 foci formation was assessed in BARD1-negative cells.

Data in (E) and (G) are presented as mean ± SD. In (C), in (D), and in (E) and (G), statistical significance was calculated using the χ^2 test for goodness of fit, Mantel-Cox test, and unpaired two-tailed Student's t test, respectively.
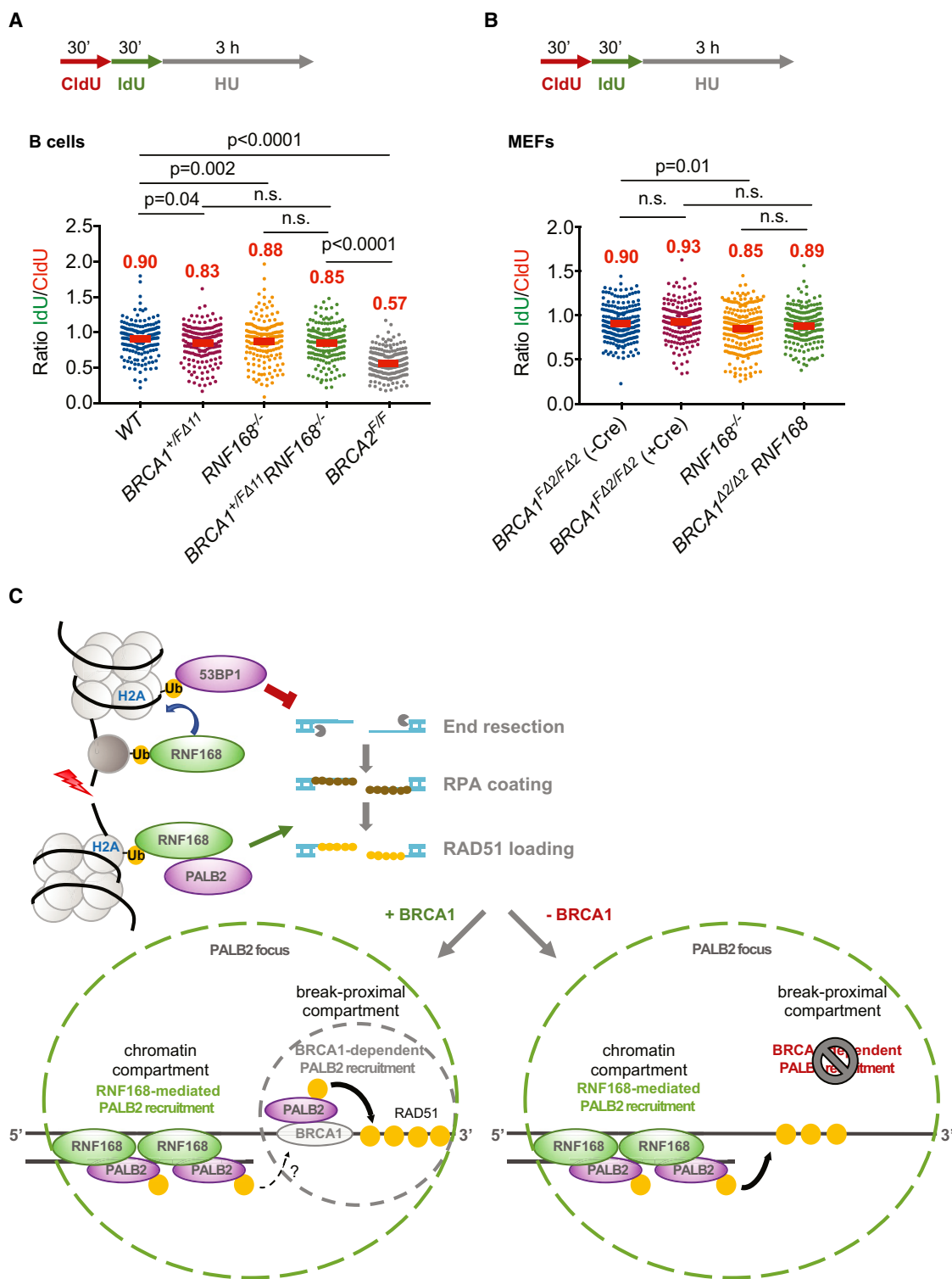
Figure 6. RNF168 Does Not Cooperate with BRCA1 in the Protection of Stalled Replication Forks

(A) Ratio of IdU versus CldU incorporation in *WT*, *BRCA1*$^{+/F\Delta11;\ CD19Cre}$, *RNF168*$^{-/-}$, and *BRCA1*$^{+/F\Delta11;\ CD19Cre}$ *RNF168*$^{-/-}$ B cells following hydroxyurea (HU) treatment. *BRCA2*$^{F/F;\ CD19Cre}$ B cells were used as a positive control for HU-induced nucleolytic degradation of nascently replicated DNA. Schematic for labeling B cells with CldU and IdU is shown at the top.

(legend continued on next page)

DSBs. Although BRCA1-directed PALB2 recruitment to ssDNA is critical for RAD51-dependent HR (Sy et al., 2009; Zhang et al., 2009a, 2009b), the physiological relevance of RNF168-mediated PALB2 chromatin loading has remained unclear (Luijsterburg et al., 2017). Based on our finding that cells become reliant on the RNF168-dependent pathway when BRCA1 protein level or its interaction with PALB2 is reduced by 50%, we suggest that ubiquitin polymers on histones assembled on ssDNA after end resection (Adkins et al., 2017; Huang et al., 2018) or surrounding the processed ssDNA compartment provide a backup mechanism to load RAD51 (Figure 6C). In BRCA1/53BP1-deficient cells, such a ubiquitin platform becomes essential to restore HR and viability. In contrast, the spread of chromatin ubiquitin conjugates around DSBs is dispensable in BRCA1 mutants that retain efficient binding to PALB2. In this case, increased resection alone is sufficient to restore HR.

Targeting Chromatin Ubiquitylation Promotes Synthetic Lethality

When HR is rewired in such a way that it becomes reliant on the chromatin ubiquitin pathway, this leads to vulnerabilities that may be targeted to induce synthetic lethality. For example, it was shown that the inhibition of ATR profoundly sensitizes PARPi-resistant BRCA1-deficient cell lines (Yazinski et al., 2017). Similarly, ATM inhibition exacerbates the HR defect in BRCA1-deficient cells (Bunting et al., 2010; Chen et al., 2017). One possibility is that, in addition to their function in promoting end resection (Cuadrado et al., 2006; Jazayeri et al., 2006; Peterson et al., 2013; Shiotani and Zou, 2009), ATM/ATR-mediated signaling of H2AX emanating from the DSB site supports RNF168 recruitment and activity, which in turn cooperates with BRCA1 to load RAD51. Consistent with this idea, it was shown that, in BRCA1-deficient cells, ATR becomes essential for BRCA2 localization (Yazinski et al., 2017). Therefore, targeting the DSB-induced chromatin ubiquitylation pathway may provide a unique therapeutic opportunity for the treatment of BRCA1-deficient cancers that become resistant to PARPi.

In addition to PARPi, proteasome inhibitors have been reported as selective BRCA1-targeting agents (Gu et al., 2014). Proteasome inhibitors profoundly impair the accumulation of RNF168, but not γ-H2AX, MDC1, or RNF8, at DNA damage sites (Doil et al., 2009; Stewart et al., 2009). Our data are therefore consistent with the idea that proteasome inhibition is synthetic lethal with BRCA1 deficiency because of the redundancy between RNF168 and BRCA1 in HR.

Deregulation of Chromatin Ubiquitylation Can Promote BRCA1 Haploinsufficiency

What triggers cancer in humans with heterozygous BRCA1 mutations remains unclear. Whereas BRCA1 heterozygosity supports HR, recent evidence indicates that mammary epithelial cells with one germline mutated BRCA1 allele exhibit genome instability and increased replication stress (Pathania et al., 2014; Sedic and Kuperwasser, 2016). Our data suggest that BRCA1 haploinsufficiency is masked by RNF168 and latent HR defects are only revealed when RNF168 levels or activity becomes lower than a certain threshold. Recent studies reveal that RNF168 protein stability is limited by the ubiquitin E3 ligases TRIP12 and UBR5 (Gudjonsson et al., 2012). Moreover, RNF168-mediated ubiquitylation signaling becomes saturated when the number of DNA breaks exceeds approximately 20 (Gudjonsson et al., 2012). Thus, if RNF168 activity is low in a few select tissues, either because of deregulated expression of RNF168 suppressors or because excessive replication stress leads to spontaneous DSBs in BRCA1 heterozygotes (Pathania et al., 2014), the resultant insufficient spreading of chromatin modifications would trigger a defect in HR, leading to genomic instability. In this way, deregulation of the chromatin ubiquitylation pathway could result in tissue-specific predisposition to cancer development in BRCA1 mutant carriers.

STAR★METHODS

Detailed methods are provided in the online version of this paper and include the following:

- KEY RESOURCES TABLE
- CONTACT FOR REAGENT AND RESOURCE SHARING
- METHOD DETAILS
  - Mice
  - Senescence-associated β-galactosidase staining
  - Cell culture
  - Generation of gene-targeted TK6 cells
  - Plasmids, transfection and viral transduction
  - Colony formation assay
  - Cell viability assay
  - Multicolor growth competition assay (MCA)
  - Metaphase spread analysis
  - Immunoblotting and immunoprecipitation
  - Immunofluorescence and laser microirradiation
  - DNA fiber assay
  - Statistics

(B) Ratio of IdU versus CldU incorporation in WT (BRCA1$^{FΔ2/FΔ2}$ no Cre), BRCA1$^{Δ2/Δ2}$ (BRCA1$^{FΔ2/FΔ2}$ + Ad-Cre), RNF168$^{−/−}$, and BRCA1$^{Δ2/Δ2}$ RNF168$^{−/−}$ MEFs following HU treatment. Schematic for labeling MEFs with CldU and IdU is shown at the top. Data shown in (A) and (B) are compiled from two independent experiments. Statistical significance was calculated using the Mann-Whitney test.

(C) A working model depicting how RNF168 cooperates with BRCA1 during HR. RNF168 regulates HR at two distinct steps. First, RNF168 recruits 53BP1 to limit end resection. Once nucleolytic processing of the break is underway, RNF168 additionally recruits PALB2 to the ssDNA compartment or chromatin flanking the break site. In BRCA1-proficient cells, loading of RAD51 is likely to be primarily carried out by the BRCA1/PALB2/BRCA2 complex that accumulates on the processed ssDNA, while RNF168/PALB2 may also assist in RAD51 assembly. As a result, loss of RNF168 in BRCA1-proficient cells produces only relatively subtle HR defects. However, if the canonical BRCA1/PALB2/BRCA2 pathway is absent or limiting in its functionality, RNF168-mediated PALB2 recruitment to ssDNA or chromatin provides an essential alternative route for RAD51 loading. Abrogation of RNF168 activity in BRCA1-compromised cells results in dramatically elevated genome instability, which may promote tumorigenesis.

AUTHOR CONTRIBUTIONS

D.Z., S.A., Y.W., H.S., E.C., M. Murga, A.D., M.J.K., N.W., M. Munro, A.R.C., and B.K. designed and performed experiments. B.X., S.T., N.J., D.D., and A.N. supervised and provided advice. D.Z. and A.N. wrote the manuscript with comments from the authors.

DECLARATION OF INTERESTS

The authors declare no competing interests.

REFERENCES

Adamson, B., Smogorzewska, A., Sigoillot, F.D., King, R.W., and Elledge, S.J. (2012). A genome-wide homologous recombination screen identifies the RNA-binding protein RBMX as a component of the DNA-damage response. Nat. Cell Biol. *14*, 318–328.

Adkins, N.L., Swygert, S.G., Kaur, P., Niu, H., Grigoryev, S.A., Sung, P., Wang, H., and Peterson, C.L. (2017). Nucleosome-like, Single-stranded DNA (ssDNA)-Histone Octamer Complexes and the Implication for DNA Double Strand Break Repair. J. Biol. Chem. *292*, 5271–5281.

Altmeyer, M., and Lukas, J. (2013). To spread or not to spread–chromatin modifications in response to DNA damage. Curr. Opin. Genet. Dev. *23*, 156–165.

Bekker-Jensen, S., Lukas, C., Kitagawa, R., Melander, F., Kastan, M.B., Bartek, J., and Lukas, J. (2006). Spatial organization of the mammalian genome surveillance machinery in response to DNA strand breaks. J. Cell Biol. *173*, 195–206.

Berton, T.R., Matsumoto, T., Page, A., Conti, C.J., Deng, C.X., Jorcano, J.L., and Johnson, D.G. (2003). Tumor formation in mice with conditional inactivation of Brca1 in epithelial tissues. Oncogene *22*, 5415–5426.

Bohgaki, T., Bohgaki, M., Cardoso, R., Panier, S., Zeegers, D., Li, L., Stewart, G.S., Sanchez, O., Hande, M.P., Durocher, D., et al. (2011). Genomic instability, defective spermatogenesis, immunodeficiency, and cancer in a mouse model of the RIDDLE syndrome. PLoS Genet. *7*, e1001381.

Bouwman, P., Aly, A., Escandell, J.M., Pieterse, M., Bartkova, J., van der Gulden, H., Hiddingh, S., Thanasoula, M., Kulkarni, A., Yang, Q., et al.

(2010). 53BP1 loss rescues BRCA1 deficiency and is associated with triple-negative and BRCA-mutated breast cancers. Nat. Struct. Mol. Biol. *17*, 688–695.

Bowman-Colin, C., Xia, B., Bunting, S., Klijn, C., Drost, R., Bouwman, P., Fineman, L., Chen, X., Culhane, A.C., Cai, H., et al. (2013). Palb2 synergizes with Trp53 to suppress mammary tumor formation in a model of inherited breast cancer. Proc. Natl. Acad. Sci. USA *110*, 8632–8637.

Bunting, S.F., and Nussenzweig, A. (2013). End-joining, translocations and cancer. Nat. Rev. Cancer *13*, 443–454.

Bunting, S.F., Callén, E., Wong, N., Chen, H.T., Polato, F., Gunn, A., Bothmer, A., Feldhahn, N., Fernandez-Capetillo, O., Cao, L., et al. (2010). 53BP1 inhibits homologous recombination in Brca1-deficient cells by blocking resection of DNA breaks. Cell *141*, 243–254.

Callen, E., Di Virgilio, M., Kruhlak, M.J., Nieto-Soler, M., Wong, N., Chen, H.T., Faryabi, R.B., Polato, F., Santos, M., Starnes, L.M., et al. (2013). 53BP1 mediates productive and mutagenic DNA repair through distinct phosphoprotein interactions. Cell *153*, 1266–1280.

Cao, L., Xu, X., Bunting, S.F., Liu, J., Wang, R.H., Cao, L.L., Wu, J.J., Peng, T.N., Chen, J., Nussenzweig, A., et al. (2009). A selective requirement for 53BP1 in the biological response to genomic instability induced by Brca1 deficiency. Mol. Cell *35*, 534–541.

Celeste, A., Petersen, S., Romanienko, P.J., Fernandez-Capetillo, O., Chen, H.T., Sedelnikova, O.A., Reina-San-Martin, B., Coppola, V., Meffre, E., Difilippantonio, M.J., et al. (2002). Genomic instability in mice lacking histone H2AX. Science *296*, 922–927.

Celeste, A., Fernandez-Capetillo, O., Kruhlak, M.J., Pilch, D.R., Staudt, D.W., Lee, A., Bonner, R.F., Bonner, W.M., and Nussenzweig, A. (2003). Histone H2AX phosphorylation is dispensable for the initial recognition of DNA breaks. Nat. Cell Biol. *5*, 675–679.

Chen, C.C., Kass, E.M., Yen, W.F., Ludwig, T., Moynahan, M.E., Chaudhuri, J., and Jasin, M. (2017). ATM loss leads to synthetic lethality in BRCA1 BRCT mutant mice associated with exacerbated defects in homology-directed repair. Proc. Natl. Acad. Sci. USA *114*, 7665–7670.

Coleman, K.A., and Greenberg, R.A. (2011). The BRCA1-RAP80 complex regulates DNA repair mechanism utilization by restricting end resection. J. Biol. Chem. *286*, 13669–13680.

Cuadrado, M., Martinez-Pastor, B., Murga, M., Toledo, L.I., Gutierrez-Martinez, P., Lopez, E., and Fernandez-Capetillo, O. (2006). ATM regulates ATR chromatin loading in response to DNA double-strand breaks. J. Exp. Med. *203*, 297–303.

Di Virgilio, M., Callen, E., Yamane, A., Zhang, W., Jankovic, M., Gitlin, A.D., Feldhahn, N., Resch, W., Oliveira, T.Y., Chait, B.T., et al. (2013). Rif1 prevents resection of DNA breaks and promotes immunoglobulin class switching. Science *339*, 711–715.

Doil, C., Mailand, N., Bekker-Jensen, S., Menard, P., Larsen, D.H., Pepperkok, R., Ellenberg, J., Panier, S., Durocher, D., Bartek, J., et al. (2009). RNF168 binds and amplifies ubiquitin conjugates on damaged chromosomes to allow accumulation of repair proteins. Cell *136*, 435–446.

Drost, R., Dhillon, K.K., van der Gulden, H., van der Heijden, I., Brandsma, I., Cruz, C., Chondronasiou, D., Castroviejo-Bermejo, M., Boon, U., Schut, E., et al. (2016). BRCA1185delAG tumors may acquire therapy resistance through expression of RING-less BRCA1. J. Clin. Invest. *126*, 2903–2918.

Escribano-Díaz, C., Orthwein, A., Fradet-Turcotte, A., Xing, M., Young, J.T., Tkáč, J., Cook, M.A., Rosebrock, A.P., Munro, M., Canny, M.D., et al. (2013). A cell cycle-dependent regulatory circuit composed of 53BP1-RIF1 and BRCA1-CtIP controls DNA repair pathway choice. Mol. Cell *49*, 872–883.

Feng, L., Fong, K.W., Wang, J., Wang, W., and Chen, J. (2013). RIF1 counteracts BRCA1-mediated end resection during DNA repair. J. Biol. Chem. *288*, 11135–11143.

Gu, Y., Bouwman, P., Greco, D., Saarela, J., Yadav, B., Jonkers, J., and Kuznetsov, S.G. (2014). Suppression of BRCA1 sensitizes cells to proteasome inhibitors. Cell Death Dis. *5*, e1580.

Gudjonsson, T., Altmeyer, M., Savic, V., Toledo, L., Dinant, C., Grøfte, M., Bartkova, J., Poulsen, M., Oka, Y., Bekker-Jensen, S., et al. (2012). TRIP12 and UBR5 suppress spreading of chromatin ubiquitylation at damaged chromosomes. Cell 150, 697–709.

Hu, Y., Scully, R., Sobhian, B., Xie, A., Shestakova, E., and Livingston, D.M. (2011). RAP80-directed tuning of BRCA1 homologous recombination function at ionizing radiation-induced nuclear foci. Genes Dev. 25, 685–700.

Huang, T.H., Fowler, F., Chen, C.C., Shen, Z.J., Sleckman, B., and Tyler, J.K. (2018). The Histone Chaperones ASF1 and CAF-1 Promote MMS22L-TONSL-Mediated Rad51 Loading onto ssDNA during Homologous Recombination in Human Cells. Mol. Cell 69, 879–892.e5.

Huen, M.S., Grant, R., Manke, I., Minn, K., Yu, X., Yaffe, M.B., and Chen, J. (2007). RNF8 transduces the DNA-damage signal via histone ubiquitylation and checkpoint protein assembly. Cell 131, 901–914.

Jazayeri, A., Falck, J., Lukas, C., Bartek, J., Smith, G.C., Lukas, J., and Jackson, S.P. (2006). ATM- and cell cycle-dependent regulation of ATR in response to DNA double-strand breaks. Nat. Cell Biol. 8, 37–45.

Kinzler, K.W., and Vogelstein, B. (1997). Cancer-susceptibility genes. Gatekeepers and caretakers. Nature 386, 761–763.

Kolas, N.K., Chapman, J.R., Nakada, S., Ylanko, J., Chahwan, R., Sweeney, F.D., Panier, S., Mendez, M., Wildenhain, J., Thomson, T.M., et al. (2007). Orchestration of the DNA-damage response by the RNF8 ubiquitin ligase. Science 318, 1637–1640.

Li, M.L., and Greenberg, R.A. (2012). Links between genome integrity and BRCA1 tumor suppression. Trends Biochem. Sci. 37, 418–424.

Li, M., Cole, F., Patel, D.S., Misenko, S.M., Her, J., Malhowski, A., Alhamza, A., Zheng, H., Baer, R., Ludwig, T., et al. (2016). 53BP1 ablation rescues genomic instability in mice expressing 'RING-less' BRCA1. EMBO Rep. 17, 1532–1541.

Ludwig, T., Chapman, D.L., Papaioannou, V.E., and Efstratiadis, A. (1997). Targeted mutations of breast cancer susceptibility gene homologs in mice: lethal phenotypes of Brca1, Brca2, Brca1/Brca2, Brca1/p53, and Brca2/p53 nullizygous embryos. Genes Dev. 11, 1226–1241.

Luijsterburg, M.S., Typas, D., Caron, M.C., Wiegant, W.W., van den Heuvel, D., Boonen, R.A., Couturier, A.M., Mullenders, L.H., Masson, J.Y., and van Attikum, H. (2017). A PALB2-interacting domain in RNF168 couples homologous recombination to DNA break-induced chromatin ubiquitylation. eLife 6, e20922.

Mailand, N., Bekker-Jensen, S., Faustrup, H., Melander, F., Bartek, J., Lukas, C., and Lukas, J. (2007). RNF8 ubiquitylates histones at DNA double-strand breaks and promotes assembly of repair proteins. Cell 131, 887–900.

Manis, J.P., Morales, J.C., Xia, Z., Kutok, J.L., Alt, F.W., and Carpenter, P.B. (2004). 53BP1 links DNA damage-response pathways to immunoglobulin heavy chain class-switch recombination. Nat. Immunol. 5, 481–487.

Mattiroli, F., Vissers, J.H., van Dijk, W.J., Ikpa, P., Citterio, E., Vermeulen, W., Marteijn, J.A., and Sixma, T.K. (2012). RNF168 ubiquitinates K13-15 on H2A/H2AX to drive DNA damage signaling. Cell 150, 1182–1195.

McCarthy, E.E., Celebi, J.T., Baer, R., and Ludwig, T. (2003). Loss of Bard1, the heterodimeric partner of the Brca1 tumor suppressor, results in early embryonic lethality and chromosomal instability. Mol. Cell Biol. 23, 5056–5063.

Messick, T.E., and Greenberg, R.A. (2009). The ubiquitin landscape at DNA double-strand breaks. J. Cell Biol. 187, 319–326.

Muñoz, M.C., Laulier, C., Gunn, A., Cheng, A., Robbiani, D.F., Nussenzweig, A., and Stark, J.M. (2012). RING finger nuclear factor RNF168 is important for defects in homologous recombination caused by loss of the breast cancer susceptibility factor BRCA1. J. Biol. Chem. 287, 40618–40628.

Nakada, S., Yonamine, R.M., and Matsuo, K. (2012). RNF8 regulates assembly of RAD51 at DNA double-strand breaks in the absence of BRCA1 and 53BP1. Cancer Res. 72, 4974–4983.

Nikkilä, J., Parplys, A.C., Pylkäs, K., Bose, M., Huo, Y., Borgmann, K., Rapakko, K., Nieminen, P., Xia, B., Pospiech, H., and Winqvist, R. (2013). Heterozygous mutations in PALB2 cause DNA replication and damage response defects. Nat. Commun. 4, 2578.

Noordermeer, S.M., Adam, S., Setiaputra, D., Barazas, M., Pettitt, S.J., Ling, A.K., Olivieri, M., Álvarez-Quilón, A., Moatti, N., Zimmermann, M., et al. (2018). The shieldin complex mediates 53BP1-dependent DNA repair. Nature 560, 117–121.

Orthwein, A., Noordermeer, S.M., Wilson, M.D., Landry, S., Enchev, R.I., Sherker, A., Munro, M., Pinder, J., Salsman, J., Dellaire, G., et al. (2015). A mechanism for the suppression of homologous recombination in G1 cells. Nature 528, 422–426.

Pathania, S., Bade, S., Le Guillou, M., Burke, K., Reed, R., Bowman-Colin, C., Su, Y., Ting, D.T., Polyak, K., Richardson, A.L., et al. (2014). BRCA1 haploinsufficiency for replication stress suppression in primary cells. Nat. Commun. 5, 5496.

Peterson, S.E., Li, Y., Wu-Baer, F., Chait, B.T., Baer, R., Yan, H., Gottesman, M.E., and Gautier, J. (2013). Activation of DSB processing requires phosphorylation of CtIP by ATR. Mol. Cell 49, 657–667.

Pilch, D.R., Sedelnikova, O.A., Redon, C., Celeste, A., Nussenzweig, A., and Bonner, W.M. (2003). Characteristics of gamma-H2AX foci at DNA double-strand breaks sites. Biochem. Cell Biol. 81, 123–129.

Polato, F., Callen, E., Wong, N., Faryabi, R., Bunting, S., Chen, H.T., Kozak, M., Kruhlak, M.J., Reczek, C.R., Lee, W.H., et al. (2014). CtIP-mediated resection is essential for viability and can operate independently of BRCA1. J. Exp. Med. 211, 1027–1036.

Prakash, R., Zhang, Y., Feng, W., and Jasin, M. (2015). Homologous recombination and human health: the roles of BRCA1, BRCA2, and associated proteins. Cold Spring Harb. Perspect. Biol. 7, a016600.

Rantakari, P., Nikkilä, J., Jokela, H., Ola, R., Pylkäs, K., Lagerbohm, H., Sainio, K., Poutanen, M., and Winqvist, R. (2010). Inactivation of Palb2 gene leads to mesoderm differentiation defect and early embryonic lethality in mice. Hum. Mol. Genet. 19, 3021–3029.

Ray Chaudhuri, A., Callen, E., Ding, X., Gogola, E., Duarte, A.A., Lee, J.E., Wong, N., Lafarga, V., Calvo, J.A., Panzarino, N.J., et al. (2016). Replication fork stability confers chemoresistance in BRCA-deficient cells. Nature 535, 382–387.

Santos, M.A., Huen, M.S., Jankovic, M., Chen, H.T., López-Contreras, A.J., Klein, I.A., Wong, N., Barbancho, J.L., Fernandez-Capetillo, O., Nussenzweig, M.C., et al. (2010). Class switching and meiotic defects in mice lacking the E3 ubiquitin ligase RNF8. J. Exp. Med. 207, 973–981.

Sasanuma, H., Tsuda, M., Morimoto, S., Saha, L.K., Rahman, M.M., Kiyooka, Y., Fujiike, H., Cherniack, A.D., Itou, J., Callen Moreu, E., et al. (2018). BRCA1 ensures genome integrity by eliminating estrogen-induced pathological topoisomerase II-DNA complexes. Proc. Natl. Acad. Sci. USA 115, E10642–E10651.

Sedic, M., and Kuperwasser, C. (2016). BRCA1-hapoinsufficiency: Unraveling the molecular and cellular basis for tissue-specific cancer. Cell Cycle 15, 621–627.

Shiotani, B., and Zou, L. (2009). Single-stranded DNA orchestrates an ATM-to-ATR switch at DNA breaks. Mol. Cell 33, 547–558.

Simhadri, S., Peterson, S., Patel, D.S., Huo, Y., Cai, H., Bowman-Colin, C., Miller, S., Ludwig, T., Ganesan, S., Bhaumik, M., et al. (2014). Male fertility defect associated with disrupted BRCA1-PALB2 interaction in mice. J. Biol. Chem. 289, 24617–24629.

Stewart, G.S., Panier, S., Townsend, K., Al-Hakim, A.K., Kolas, N.K., Miller, E.S., Nakada, S., Ylanko, J., Olivarius, S., Mendez, M., et al. (2009). The RIDDLE syndrome protein mediates a ubiquitin-dependent signaling cascade at sites of DNA damage. Cell 136, 420–434.

Stucki, M., Clapperton, J.A., Mohammad, D., Yaffe, M.B., Smerdon, S.J., and Jackson, S.P. (2005). MDC1 directly binds phosphorylated histone H2AX to regulate cellular responses to DNA double-strand breaks. Cell 123, 1213–1226.

Sy, S.M., Huen, M.S., and Chen, J. (2009). PALB2 is an integral component of the BRCA complex required for homologous recombination repair. Proc. Natl. Acad. Sci. USA 106, 7155–7160.

Tan, S.L.W., Chadha, S., Liu, Y., Gabasova, E., Perera, D., Ahmed, K., Constantinou, S., Renaudin, X., Lee, M., Aebersold, R., and Venkitaraman, A.R. (2017). A Class of Environmental and Endogenous Toxins Induces BRCA2 Haploinsufficiency and Genome Instability. Cell *169*, 1105–1118.e15.

Thorslund, T., Ripplinger, A., Hoffmann, S., Wild, T., Uckelmann, M., Villumsen, B., Narita, T., Sixma, T.K., Choudhary, C., Bekker-Jensen, S., and Mailand, N. (2015). Histone H1 couples initiation and amplification of ubiquitin signalling after DNA damage. Nature *527*, 389–393.

Tutt, A., and Ashworth, A. (2002). The relationship between the roles of BRCA genes in DNA repair and cancer predisposition. Trends Mol. Med. *8*, 571–576.

Wang, Y., Bernhardy, A.J., Cruz, C., Krais, J.J., Nacson, J., Nicolas, E., Peri, S., van der Gulden, H., van der Heijden, I., O'Brien, S.W., et al.; kConFab Investigators (2016a). The BRCA1-Δ11q Alternative Splice Isoform Bypasses Germline Mutations and Promotes Therapeutic Resistance to PARP Inhibition and Cisplatin. Cancer Res. *76*, 2778–2790.

Wang, Y., Krais, J.J., Bernhardy, A.J., Nicolas, E., Cai, K.Q., Harrell, M.I., Kim, H.H., George, E., Swisher, E.M., Simpkins, F., and Johnson, N. (2016b). RING domain-deficient BRCA1 promotes PARP inhibitor and platinum resistance. J. Clin. Invest. *126*, 3145–3157.

Ward, I.M., Minn, K., van Deursen, J., and Chen, J. (2003). p53 Binding protein 53BP1 is required for DNA damage responses and tumor suppression in mice. Mol. Cell. Biol. *23*, 2556–2563.

Ward, I.M., Reina-San-Martin, B., Olaru, A., Minn, K., Tamada, K., Lau, J.S., Cascalho, M., Chen, L., Nussenzweig, A., Livak, F., et al. (2004). 53BP1 is required for class switch recombination. J. Cell Biol. *165*, 459–464.

Wilson, M.D., Benlekbir, S., Fradet-Turcotte, A., Sherker, A., Julien, J.P., McEwan, A., Noordermeer, S.M., Sicheri, F., Rubinstein, J.L., and Durocher, D. (2016). The structural basis of modified nucleosome recognition by 53BP1. Nature *536*, 100–103.

Xie, A., Puget, N., Shim, I., Odate, S., Jarzyna, I., Bassing, C.H., Alt, F.W., and Scully, R. (2004). Control of sister chromatid recombination by histone H2AX. Mol. Cell *16*, 1017–1025.

Xie, A., Hartlerode, A., Stucki, M., Odate, S., Puget, N., Kwok, A., Nagaraju, G., Yan, C., Alt, F.W., Chen, J., et al. (2007). Distinct roles of chromatin-associated proteins MDC1 and 53BP1 in mammalian double-strand break repair. Mol. Cell *28*, 1045–1057.

Xu, X., Qiao, W., Linke, S.P., Cao, L., Li, W.M., Furth, P.A., Harris, C.C., and Deng, C.X. (2001). Genetic interactions between tumor suppressors Brca1 and p53 in apoptosis, cell cycle and tumorigenesis. Nat. Genet. *28*, 266–271.

Yazinski, S.A., Comaills, V., Buisson, R., Genois, M.M., Nguyen, H.D., Ho, C.K., Todorova Kwan, T., Morris, R., Lauffer, S., Nussenzweig, A., et al. (2017). ATR inhibition disrupts rewired homologous recombination and fork protection pathways in PARP inhibitor-resistant BRCA-deficient cancer cells. Genes Dev. *31*, 318–332.

Zhang, F., Fan, Q., Ren, K., and Andreassen, P.R. (2009a). PALB2 functionally connects the breast cancer susceptibility proteins BRCA1 and BRCA2. Mol. Cancer Res. *7*, 1110–1118.

Zhang, F., Ma, J., Wu, J., Ye, L., Cai, H., Xia, B., and Yu, X. (2009b). PALB2 links BRCA1 and BRCA2 in the DNA-damage response. Curr. Biol. *19*, 524–529.

Zhang, F., Bick, G., Park, J.Y., and Andreassen, P.R. (2012). MDC1 and RNF8 function in a pathway that directs BRCA1-dependent localization of PALB2 required for homologous recombination. J. Cell Sci. *125*, 6049–6057.

Zimmermann, M., Lottersberger, F., Buonomo, S.B., Sfeir, A., and de Lange, T. (2013). 53BP1 regulates DSB repair using Rif1 to control 5′ end resection. Science *339*, 700–704.

Zong, D., Callén, E., Pegoraro, G., Lukas, C., Lukas, J., and Nussenzweig, A. (2015). Ectopic expression of RNF168 and 53BP1 increases mutagenic but not physiological non-homologous end joining. Nucleic Acids Res. *43*, 4950–4961.

STAR★METHODS

KEY RESOURCES TABLE

REAGENT or RESOURCE	SOURCE	IDENTIFIER
Antibodies		
Rabbit polyclonal anti-53BP1	Novus Biologicals	Cat# NB100-305; RRID: AB_10001695
Rabbit polyclonal anti-53BP1	EMD Millipore	Cat# PC712; RRID: AB_564982
Rabbit polyclonal anti-BARD1	Richard Baer (McCarthy et al., 2003)	N/A
Mouse monoclonal anti-BRCA1	R&D Systems	N/A, Custom-made
Rabbit polyclonal anti-BRCA2	Bethyl Laboratories	Cat# A303-434A; RRID: AB_10952240
Rabbit polyclonal anti-BRCC36	Bethyl Laboratories	Cat# A302-517A; RRID: AB_1966097
Mouse monoclonal anti-BrdU (B44)	BD Biosciences	Cat# 347580; RRID: AB_400326
Rat monoclonal anti-BrdU (BU1/75 (ICR1))	Abcam	Cat# Ab6326; RRID: AB_305426
Rabbit polyclonal anti-CENPF	Abcam	Cat# Ab5; RRID: AB_304721
Mouse monoclonal anti-Cyclin A2 (E23.1)	Abcam	Cat# Ab38; RRID: AB_304084
Mouse monoclonal anti-GFP	Roche Applied Science	Cat# 11814460001; RRID: AB_390913
Mouse monoclonal anti-FLAG (M2)	Sigma-Aldrich	Cat# F1804; RRID: AB_262044
Rabbit polyclonal anti-H2AX (pS139)	Novus Biologicals	Cat# NB100-384; RRID: AB_10002815
Mouse monoclonal anti-HA (6E2)	Cell Signaling Technology	Cat# 2367; RRID: AB_10691311
Rabbit polyclonal anti-PALB2	Bethyl Laboratories	Cat# A301-247A; RRID: AB_890608
Rabbit polyclonal anti-RAD51 (H-92)	Santa Cruz Biotechnology	Cat# sc-8349; RRID: AB_2253533
Mouse monoclonal anti-RAD51 (G-9)	Santa Cruz Biotechnology	Cat# sc-377467
Rabbit polyclonal anti-RAD51	Bio Academia	Cat# 70-001; RRID: AB_2177110
Sheep polyclonal anti-RNF168	R&D Systems	Cat# AF7217
Rabbit polyclonal anti-RNF168	EMD Millipore	Cat# ABE367; RRID: AB_11205761
Rat monoclonal anti-RPA2 (4E4)	Cell Signaling Technology	Cat# 2208; RRID: AB_2238543
Rabbit polyclonal anti-RPA2 (pS4, S8)	Bethyl Laboratories	Cat# A300-245A; RRID: AB_210547
Mouse monoclonal anti-α-Tubulin	Sigma-Aldrich	Cat# T-5168; RRID: AB_477579
ECL Sheep anti-Mouse IgG HRP-linked whole antibody	GE Healthcare	Cat# NXA931
ECL Donkey anti-Rabbit IgG HRP-linked F(ab')$_2$	GE Healthcare	Cat# NA9340V
IRDye 680RD Goat anti-Mouse IgG (H+L)	LI-COR Biosciences	Cat# 925-68070
IRDye 800CW Goat anti-Mouse IgG (H+L)	LI-COR Biosciences	Cat# 926-32210
IRDye 680RD Goat anti-Rabbit IgG (H+L)	LI-COR Biosciences	Cat# 925-68071
IRDye 800CW Goat anti-Rabbit IgG (H+L)	LI-COR Biosciences	Cat# 925-32211
Alexa Fluor 488 Goat anti-Mouse IgG (H+L)	Thermo Fisher Scientific	Cat# A11001
Alexa Fluor 568 Goat anti-Mouse IgG (H+L)	Thermo Fisher Scientific	Cat# A11031
Alexa Fluor 568 Goat anti-Rat IgG (H+L)	Thermo Fisher Scientific	Cat# A11077
Alexa Fluor 488 Chicken anti-Rabbit IgG (H+L)	Thermo Fisher Scientific	Cat# A21441
Alexa Fluor 568 Goat anti-Rabbit IgG (H+L)	Thermo Fisher Scientific	Cat# A11011
Alexa Fluor 568 Donkey anti-Sheep IgG (H+L)	Thermo Fisher Scientific	Cat# 21099
Cy3 Donkey anti-Rat IgG (H+L)	Jackson ImmunoResearch	Cat# 712-166-153
Purified Rat anti-Mouse CD180 (RP/14)	BD Biosciences	Cat# 552128
Purified Rat anti-Mouse CD16/CD32 (2.4G2) Fc Block	BD Biosciences	Cat# 553141
Biotin Rat anti-Mouse IgG1 (A85-1)	BD Biosciences	Cat# 553441
FITC Rat anti-Mouse B220 (RA3-6B2)	BD Biosciences	Cat# 553088
Bacterial and Virus Strains		
Bacteria: TOP10 Chemically Competent *E. coli*	Thermo Fisher Scientific	Cat# C404006
Bacteria: STBL3 Chemically Competent *E. coli*	Thermo Fisher Scientific	Cat# C737303

(Continued on next page)

REAGENT or RESOURCE	SOURCE	IDENTIFIER
Retrovirus: pCL-ECO	Addgene	Cat# 12371
Retrovirus: pMX-empty-IRES-GFP-Puro	Jiri Lukas, Zong et al., 2015	N/A
Retrovirus: pMX-RNF168(WT)-IRES-GFP-Puro	Jiri Lukas, Zong et al., 2015	N/A
Retrovirus: pMX-RNF168(R57D)-IRES-GFP-Puro	Jiri Lukas, Zong et al., 2015	N/A
Retrovirus: pMX-empty(no IRES-GFP)-Puro	Gift from Davide Robbiani	N/A
Retrovirus: pMX-GFP-PALB2-Puro	This paper	N/A
Retrovirus: pMX-GFP-FHA(RNF8)-PALB2-Puro	This paper	N/A
Lentivirus: pLenti-BRCA1(WT)-IRES-GFP	Wang et al., 2016a, 2016b	N/A
Lentivirus: pLenti-BRCA1(ΔRING)-IRES-GFP	Wang et al., 2016b	N/A
Lentivirus: pLenti-BRCA1(Δ11q)-IRES-GFP	Wang et al., 2016a	N/A
Adenovirus: Ad5-CMV-eGFP	Addgene	N/A
Adenovirus: Ad5-CMV-Cre-eGFP	Addgene	N/A
Chemicals, Peptides, and Recombinant Proteins		
Olaparib	Selleckchem	Cat# AZD2281
Cisplatin	Sigma-Aldrich	Cat# 479306
Hydroxyurea	Sigma-Aldrich	Cat# H8627
Lipopolysaccharide (LPS) from *E. coli* O111:B4	Sigma-Aldrich	Cat# L2630
Interleukin 4 (IL-4) from mouse	Sigma-Aldrich	Cat# I1020
CD43 microbeads (Ly-48)	Miltenyi Biotec	Cat# 130-049-801
Protein G Magnetic Beads	Active Motif	Cat# 104502
X-tremeGENE 9 DNA Transfection Reagent	Roche Diagnostics	Cat# 6365809001
GeneArt Seamless Cloning Enzyme Mix	Thermo Fisher Scientific	
Zero Blunt PCR Cloning Kit	Thermo Fisher Scientific	Cat# K270020
PNA probe for telomeres Cy3-(CCCTAA)$_3$	PNA Bio	Cat# F1002
DAPI	Thermo Fisher Scientific	Cat# 62248
EdU	Thermo Fisher Scientific	Cat# A10044
IdU	Sigma-Aldrich	Cat# I7125
CldU	Sigma-Aldrich	Cat# C6891
Colcemid	Roche Diagnostics	Cat# 10295892001
Hoechst 33342	Thermo Fisher Scientific	Cat# 62249
PE Streptavidin	BD Biosciences	Cat# 554061
Crystal Violet	Sigma-Aldrich	Cat# 0775
3-Indoleacetic acid (Auxin)	Sigma-Aldrich	Cat# I3750
Critical Commercial Assays		
Click-IT EdU Alexa Fluor 488 Flow Cytometry Assay Kit	Thermo Fisher Scientific	Cat# C10425
Click-IT EdU Alexa Fluor 647 Flow Cytometry Assay Kit	Thermo Fisher Scientific	Cat# C10634
Senescence β-Galactosidase Staining Kit	Cell Signaling Technology	Cat# 9860
CellTiter-Glo Luminescent Cell Viability Assay	Promega	Cat# G7571
NE-PER Nuclear and Cytoplasmic Extraction Reagents	Thermo Fisher Scientific	Cat# 78833
Pierce Classic IP Kit	Thermo Fisher Scientific	Cat# 26146
Experimental Models: Cell Lines		
Embryonic stem cell: RNF168$^{-/-}$ (JM8A3.N1.C2)	International Knockout Mouse Consortium	Rnf168$^{tm2a(EUCOMM)Hmgu}$
MEF: Wildtype	This paper	N/A
MEF: BRCA1$^{+/\Delta 11}$	This paper	N/A
MEF: RNF168$^{-/-}$	This paper	N/A
MEF: BRCA1$^{+/\Delta 11}$ RNF168$^{-/-}$	This paper	N/A
MEF: BRCA1$^{F2/F2}$	This paper	N/A

Continued

REAGENT or RESOURCE	SOURCE	IDENTIFIER
MEF: BRCA1$^{\Delta 2/\Delta 2}$ RNF168$^{-/-}$	This paper	N/A
MEF: BRCA1$^{\Delta 2/\Delta 2}$ 53BP1$^{-/-}$	Bunting	N/A
hTERT-RPE1: BRCA1$^{-/-}$ 53BP1$^{-/-}$ p53$^{-/-}$ (+FLAG-Cas9)	Noordermeer et al., 2018	N/A
TK6: Wildtype (+TIR1)	Sasanuma et al., 2018	N/A
TK6: BRCA1$^{AID/AID}$ (+TIR1)	Sasanuma et al., 2018	N/A
TK6: BRCA1$^{AID/AID}$ RNF168$^{-/-}$ (+TIR1)	This paper	N/A
TK6: 53BP1$^{-/-}$ (+TIR1)	Sasanuma et al., 2018	N/A
TK6: BRCA1$^{AID/AID}$ 53BP1$^{-/-}$ (+TIR1)	Sasanuma et al., 2018	N/A
MDA-MD-436	ATCC	ATCC HTB-130
Experimental Models: Organisms/Strains		
Mouse: BRCA1$^{F\Delta 11/F\Delta 11}$CD19Cre. B6/129	NCI mouse repository	Strain # 01XC8
Mouse: BRCA1$^{+/\Delta 11}$. B6/129	NCI mouse repository	Strain # 01XC9
Mouse: RNF168$^{-/-}$. B6	This paper	N/A
Mouse: 53BP1$^{-/-}$. B6/129	Ward et al., 2003	N/A
Mouse: RNF8$^{-/-}$. B6/129	Santos et al., 2010	N/A
Mouse: p53$^{+/-}$. B6/129	Taconic Biosciences	N/A
Mouse: H2AX$^{-/-}$. B6/129	Celeste et al., 2002	N/A
Mouse: BRCA2$^{F/F}$. B6/129	NCI mouse repository	Strain # 01XB9
Mouse: PALB2$^{CC6/CC6}$. B6/129	Simhadri et al., 2014	N/A
Mouse: BRCA1$^{F\Delta 2/F\Delta 2}$CD19Cre. B6/129	Li et al., 2016	N/A
Mouse: BRCA1$^{+/\Delta 2}$. B6/129	Ludwig et al., 1997	N/A
Oligonucleotides		
Primers for genotyping WT *RNF168* allele: Forward, 5′-CAAGGAAACAAACAGCGTTAGGGC; Reverse, 5′-CAACGGGTTCTTCTGTTAGTCC	This paper	N/A
Primers for genotyping WT *RNF168* allele: Forward, 5′-TGACATTCCACACCACTTTCTAGC; Reverse, 5′-CAACGGGTTCTTCTGTTAGTCC	This paper	N/A
sgRNAs targeting endogenous human RNF168 locus (TK6): #1: 5′-ACTGGCACTCGGACAGCGAG; #2: 5′-GGAGGGTGACGGGCTCCACG	This paper	N/A
RNF168 targeting vector construction; left homology arm forward primer, 5′-GCGAATTGGGTACCGGGCC GCCTGGATAAAACAGTGAGACCCCA	This paper	N/A
RNF168 targeting vector construction; left homology arm reverse primer, 5′-CTGGGCTCGAGGGGGGGC CGGCGTCTTTGGGTAGAGCCATTTCA	This paper	N/A
RNF168 targeting vector construction; right homology arm forward primer, 5′-TGGGAAGCTTGTCGACTTAA TCGAAAAGGCGAGTTTATGCTGTC	This paper	N/A
RNF168 targeting vector construction; right homology arm reverse primer, 5′-CACTAGTAGGCGCGCCTT AAGCTTATTGCTCACATTAGTGGAGG	This paper	N/A
sgRNA targeting endogenous human BRCA1 locus (TK6): 5′- GGAGTCGATTGATTAGA	Sasanuma et al., 2018	N/A
Recombinant DNA		
Plasmid: FLAG-PALB2	Orthwein et al., 2015	N/A
Plasmid: GFP-PALB2	Orthwein et al., 2015	N/A
Plasmid: pX330	Addgene	Cat# 42230
Plasmid: pCMV-SV40T	Gift from Kai Ge	N/A

(Continued on next page)

Continued

REAGENT or RESOURCE	SOURCE	IDENTIFIER
Software and Algorithms		
ZEN 2 (blue edition)	Zeiss	https://www.zeiss.com/corporate/int/home.html
Metafer 4	MetaSystems	https://metasystems-international.com/
Acapella script (custom)	PerkinElmer	https://www.perkinelmer.com/
Prism 8	GraphPad	https://www.graphpad.com/
ImageJ	National Institutes of Health	https://imagej.nih.gov/ij
RStudio	RStudio Team	https://www.rstudio.com/
FlowJo (10.1)	FlowJo LLC	https://www.flowjo.com/
Other		
BOSC23 retrovirus packaging cells	ATCC	CRL-11270; RRID: CVCL_4401
Glass Bottom Microwell Dishes	MatTek Corporation	Cat# P35G-1.5-14-C
FluoroBrite DMEM Media	Thermo Fisher Scientific	Cat# A1896701
LSM510 confocal microscope	Zeiss	N/A
Axio Observer Z1 epifluorescence microscope	Zeiss	N/A
IN Cell Analyzer	GE Healthcare	N/A
Odyssey CLx Imaging System	LI-COR Biosciences	N/A
FACSCalibur	BD Biosciences	N/A
Cytogenetic drying chamber	Thermotron	N/A
Nano Quant Infinite M200 Pro microplate reader	Tecan	N/A
Mark 1 ^{137}Cs irradiator	JL Shepherd	N/A

CONTACT FOR REAGENT AND RESOURCE SHARING

As Lead Contact, André Nussenzweig is responsible for all reagent and resource requests. Please contact André Nussenzweig at andre_nussenzweig@nih.gov with requests and inquiries.

METHOD DETAILS

Mice

The embryonic stem cell line JM8A3.N1.C2 was used to generate RNF168 deficient mice at the Transgenic Mouse Model Laboratory (Frederick National Laboratory for Cancer Research). Three derivative clones (HEPD0798_7_D9, HEPD0798_7_B10, HEPD0798_7_F12) (Toronto Centre for Phenogenomics), in which the *RNF168* gene was disrupted by insertion of a neomycin gene selection cassette into exon 2, were injected into C57BL/6 blastocysts. The resultant chimeric offspring were backcrossed with wild-type C57BL/6 mice, producing *RNF168*$^{+/-}$ animals. Germline transmission of the targeted allele was confirmed by PCR (forward, 5′-TGACATTCCACACCACTTTCTAGC; reverse, 5′-CAACGGGTTCTTCTGTTAGTCC) in DNA extracted from tail clips and an alternate (5′-CAAGGAAACAAACAGCGTTAGGGC) reverse primer was used to amplify the non-targeted wild-type allele. Finally, heterozygotes were further intercrossed to generate homozygous RNF168$^{-/-}$ mice.

BRCA1$^{+/\Delta 11}$ (germline), *BRCA1*$^{F\Delta 11/F\Delta 11; \ CD19Cre}$, *BRCA2*$^{F/F; \ CD19Cre}$ (conditional) mice were obtained from the NCI mouse repository. *P53*$^{+/-}$ mice were obtained from Taconic Biosciences. *BRCA1*$^{\Delta 11/F\Delta 11; \ CD19Cre}$ mice were generated by crossing *BRCA1*$^{F\Delta 11/F\Delta 11; \ CD19Cre}$ mice with *BRCA1*$^{+/\Delta 11}$ mice. Germline *BRCA1*$^{+/\Delta 2}$ and conditional *BRCA1*$^{F\Delta 2/F\Delta 2; \ CD19Cre}$ mice were kindly provided by Dr. Thomas Ludgwid. *53BP1*$^{-/-}$, *H2AX*$^{-/-}$, *RNF8*$^{-/-}$, *PALB2*$^{CC6/CC6}$ mice have been described (Celeste et al., 2002; Santos et al., 2010; Simhadri et al., 2014; Ward et al., 2003). All breeding and experimentation involving mice followed protocols approved by the National Institutes of Health Institutional Animal Care and Use Committee.

Senescence-associated β-galactosidase staining

Mouse embryos were extracted on day E16.5 following timed pregnancies and fixed in 2% formaldehyde and 0.2% glutaraldehyde for 45 min. After thorough washing in PBS, the fixed embryos were stained for senescence associated β-galactosidase activity using a commercially available kit (Cell Signaling Technology), as per manufacturer's instructions.

Cell culture

Mouse embryonic fibroblasts

To isolate primary mouse embryonic fibroblasts (MEFs), E13.5 embryos were first minced with scissors and then trypsinized. The liberated cells were incubated in Dulbecco's Modified Eagle's Medium (DMEM, GIBCO) supplemented with 15% heat-inactivated fetal bovine serum (FBS, Gemini Bio-Products) and 1% penicillin + streptomycin (GIBCO). For growth assays, 100,000 primary MEFs from passages 3-4 are plated in triplicate 60 mm dishes. Cell numbers were recorded on consecutive days for seven (*WT*, *RNF168*$^{-/-}$, *BRCA1*$^{+/\Delta 11}$) or fourteen days (*BRCA1*$^{\Delta 11/\Delta 11}$, *BRCA1*$^{+/\Delta 11}$*RNF168*$^{-/-}$).

To establish immortalized MEF cell lines, primary MEFs between passages 2-4 were transiently transfected with a vector encoding SV40 T-antigen (pCMV-SV40T). SV40-immortalized MEFs were routinely cultured in DMEM supplemented with 10 or 15% FBS.

Mouse B cells

Resting primary B cells were isolated from the spleen using anti-CD43 microbeads (Miltenyi Biotec). Purified cells were resuspended in complete B cell medium containing 25 µg/mL LPS, 5 ng/mL IL-4 (both Sigma-Aldrich) and 0.5 µg/mL anti-CD180 (BD Biosciences) to stimulate proliferation and immunoglobulin class switch recombination (CSR). Successful *ex vivo* CSR was assayed on day 3 by flow cytometry following live cell staining using biotinylated anti-IgG1 and FITC conjugated anti-B220 antibodies (BD Biosciences). Analysis of FACS data was done using FlowJo (version 10).

Human cell lines

TK6 cells were grown in RPMI-1640 GlutaMax medium supplemented with 10% horse serum (both from GIBCO). RPE1 cells were cultured in DMEM supplemented with 10% FBS. All culture medium contained 1% penicillin + streptomycin.

Generation of gene-targeted TK6 cells

To construct targeting vectors for the endogenous *BRCA1* locus (Sasanuma et al., 2018), the left and right homology arms were amplified using the following sets of primers: left arm-F, 5′-AGGGCGAATTGGAGCTCCCCCAGATTGAAGTTCATGTTAATACAG and left arm-R, 5′-TTGGCGCCTGCACCGGATCCGTAGTGGCTGTGGGGGATCTGGGGT; right arm-F, 5′-CGAAGTTATTAGGT CCCTCGTAGTCCAGGAGAATGAATTGACACT and right arm-R, 5′-GGGAACAAAAGCTGGGGAACCTCTTCTCACTGTCACCCAGG CTGGAGTGC. The guide RNA (gRNA) recognition sequence (5′-GGAGTCGATTGATTAGA) was removed from the left homology arm to prevent unwanted digestion by CRISPR-Cas9. Both homology arms were subsequently assembled into each of two vectors encoding the auxin-inducible degron (AID), pBS-mAID-GFP-loxP-NEO^R (digested with EcoNI/SmaI) and pBS-mAID-GFP-loxP-HIS^R (digested with EcoNI/BamHI), respectively, using the GeneArt Seamless Cloning Enzyme Mix (Thermo Fisher). The gRNA was inserted into the BbsI site of pX330 (Addgene). The resulting pX330-gRNA vector was co-transfected along with the *BRCA1* targeting vectors into *WT* and *53BP1*$^{-/-}$ TK6 cells expressing the *TIR1* ubiquitin ligase gene (Sasanuma et al., 2018).

To construct targeting vectors for the *RNF168* gene, the left and right homology arms (∼1 kb) were amplified using the following sets of primers: left arm-F, 5′-GCGAATTGGGTACCGGGCCGCCTGGATAAAACAGTGAGACCCCA and left arm-R, 5′-CTGGGGCT CGAGGGGGGGGCCGGCGTCTTTGGGTAGAGCCATTTCA; right arm-L, 5′-TGGGAAGCTTGTCGACTTAATCGAAAAGGCGAGTT TATGCTGTC and right arm-R, 5′-CACTAGTAGGCGCGCCTTAAGCTTATTGCTCACATTAGTGGAGG. Both homology arms were assembled into each of two ApaI/AflII-digested expression vectors, pDT-ApA/HYGRO^R and pDT-ApA/BSR^R, respectively, using the GeneArt Seamless Cloning Enzyme Mix. Two gRNAs targeting *RNF168* (5′-ACTGGCACTCGGACAGCGAG; 5′-GGAGGGT GACGGGCTCCACG) were individually inserted into the BbsI site of pX330. The resulting pX330-gRNA vectors were co-transfected along with the *RNF168* targeting vectors into *BRCA1*$^{AID/AID}$ TK6 cells. After transfection, cells were released into 20 mL drug-free medium containing 10% horse serum. Forty-eight hours after transfection, cells were seeded into 96-well plates and grown in medium containing hygromycin and blasticidin for two weeks. Surviving single cell-derived clones were validated for homozygous gene targeting by PCR using the following primers: HYGRO^R_F (5′-ATCTTTGTAGAAACCATCGGCGCAGCTATT)/BSR^R_F (5′-GAATT GCCGCTCCCACATGATGTTTATTAT) and RNF168_CHK_R (5′-CACGAGAGAACGGAGACACCATATCCTAAG).

To induce degradation of AID-tagged BRCA1 protein, auxin (3-indoleacetic acid, Sigma-Aldrich) was added to the cell culture medium (500 µM final concentration). For growth assay, cell numbers were recorded for seven consecutive days.

Plasmids, transfection and viral transduction

Retroviral pMX-PIE-based vectors encoding wild-type human RNF168 and the catalytic dead (R57D) mutant have been described (Zong et al., 2015). cDNA corresponding to wild-type human PALB2 was amplified by PCR from pDEST-FRT-TO-GFP-PALB2 (Orthwein et al., 2015), and subcloned into the multiple cloning site of pMX (no IRES-GFP), producing pMX-GFP-PALB2. Retroviral vector encoding PALB2^{FHA} was produced by PCR amplification of the FHA domain of RNF8 from pMX-RNF8(FHA)-RNF168 and subcloned into pMX-GFP-PALB2 between GFP and PALB2. Infection-competent retroviral particles were assembled in BOSC23 cells co-transfected with the pCL-ECO helper virus. Retroviral supernatant was collected 40–48 h later to transduce MEFs and B cells.

Pre-made adenovirus (Ad5-CMV-GFP and Ad5-CMV-Cre-GFP, Addgene) was used at a MOI of 100 to transduce MEFs.

Mammalian expression vectors encoding GFP-tagged PALB2 (pDEST-FRT-TO-GFP-PALB2), FLAG-tagged PALB2 (pDEST-FRT-TO-FLAG-PALB2) have been described (Orthwein et al., 2015). Transient expression was achieved by transfection in MEFs using the X-tremeGENE 9 DNA transfection reagent (Roche Diagnostics), as per manufacturer's instructions.

Colony formation assay

Cells were treated with indicated doses of the PARP inhibitor Olaparib (Selleckchem) or cisplatin (Sigma-Aldrich) continuously for 10 days (Olaparib) or for 24 h followed by a 9-day post-incubation in drug-free medium (cisplatin). Thereafter, culture dishes were stained with 0.5% crystal violet and colonies containing > 50 cells were tallied.

Cell viability assay

Twenty-four hours post cytokine stimulation, primary activated B cells were treated with either vehicle, 1 μM PARPi or 0.5 μM cisplatin continuously for 48 h. Thereafter, cell viability was determined using the CellTiter-Glo Luminescent Cell Viability Assay (Promega) as per manufacturer's instructions.

Multicolor growth competition assay (MCA)

Generation of hTERT-RPE1 $BRCA1^{-/-}53BP1^{-/-}p53^{-/-}$ FLAG-Cas9 cells has been described (Noordermeer et al., 2018). One hundred thousand cells were infected at an MOI of ~1.2 to ensure 100% transduction efficiency with either virus particles of NLS-mCherry LacZ-sgRNA or NLS-GFP GOI-sgRNA (RNF168, PALB2, BRCA2 or the empty vector). Ninety-six hours after transduction, mCherry- and GFP-expressing cells were mixed 1:1 (3,000 cells + 3,000 cells) and seeded in 12-well plates. During the course of the experiment, cells were subcultured when near confluency was reached. Cells were imaged for GFP- and mCherry signal the day of initial plating (t = 0) and on days 3, 7, 10, 14 and 17 using the automated IN Cell Analyzer (GE Healthcare Life Sciences) with a 4X objective. An Acapella script (PerkinElmer) was used to segment and quantify the number of GFP-positive and mCherry-positive cells. Efficiency of indel formation was determined by PCR amplification of the region surrounding the sgRNA sequence and TIDE analysis on DNA isolated from GFP-expressing cells 6 days post-transduction.

Metaphase spread analysis

Activated cycling B cells and asynchronous MEFs were treated with 1 μM PARPi (24 h) or 0.5 μM cisplatin (18 h) and subsequently arrested at mitosis with colcemid (Invitrogen). Cells were incubated in pre-warmed KCl (Sigma-Aldrich, 75 mM) for 20 minutes in a 37°C water bath to induce swelling and then fixed in methanol/glacial acetic acid (ratio 3:1). Droplets of cells were spread onto glass slides inside a cytogenetic drying chamber (Thermotron). Fluorescence *in situ* hybridization was performed with a Cy3-labeled (CCCTAA)$_3$ peptide nucleic acid probe (PNA Bio) to stain telomeres, and DNA was counterstained with DAPI (Callen et al., 2013). Images were captured with the Metafer automated scanning and imaging platform (MetaSystems). One hundred metaphases were scored for the presence of chromosomal aberrations.

Immunoblotting and immunoprecipitation

For immunoblotting, cells were lysed in a buffer containing 50 mM Tris-HCl (pH 7.5), 200 mM NaCl, 5% Tween-20, 2% Igepal CA-630, 2 mM PMSF, 50 mM β-glycerophosphate (all from Sigma-Aldrich) and protease inhibitor cocktail tablet (cOmplete Mini, Roche Diagnostics). Equal amounts of lysates were loaded into precast mini-gels (Invitrogen) and resolved by SDS-PAGE. Transfer of proteins onto nitrocellulose membranes and incubation with primary/secondary antibodies were performed according to standard procedures. Visualization of protein bands was achieved by either enhanced chemiluminescence (Amersham) or fluorescence imaging (LI-COR Biosciences).

For co-immunoprecipitation experiments, mCherry (mCh), BRCA1-full-length (FL), BRCA1-ΔRING (del aa1-127) and BRCA1-Δ11q (del aa264-1366) proteins were ectopically expressed in MD-MBA-436 cells (Wang et al., 2016a; Wang et al., 2016b). Nuclear extracts were prepared using NE-PER Nuclear and Cytoplasmic Extraction Reagents (Thermo Fisher Scientific) according to manufacturer's instructions. HA antibody was then used to pull down tagged BRCA1 complexes from 3 mg of nuclear extract using Pierce Classic IP Kit (Thermo Fisher Scientific). Because ectopic BRCA-Δ11q was expressed at significantly higher levels than BRCA1-FL and BRCA1-ΔRING, different volumes of IP elution were loaded in protein mini-gels in order to achieve similar loading of all three BRCA1 isoforms. Samples were subsequently resolved by standard SDS-PAGE. BRCA1 binding partners were detected by antibodies recognizing BRCA2, PALB2, and RAD51.

Immunofluorescence and laser microirradiation

For immunofluorescence staining, cells grown on coverslips were first incubated in culture medium containing 10 μM EdU (Invitrogen) for 20 min prior to γ-irradiation (^{137}Cs Mark 1) (JL Shepherd). Thereafter, cells were pre-extracted (20 mM HEPES, 50 mM NaCl, 3 mM MgCl$_2$, 0.3 M sucrose, 0.2% Triton X-100) on ice for 5 min to remove soluble nuclear proteins. Extracted samples were fixed (4% paraformaldehyde), permeabilized (0.5% Triton X-100), incubated with appropriate primary antibodies followed by appropriate fluorochrome-conjugated secondary antibodies (Invitrogen). Next, click-IT chemistry was performed as per manufacturer's instructions and DNA was counterstained with DAPI (Thermo Fisher Scientific). Images were captured at 63X magnification with an AxioCam MRc5 mounted on an Axio Observer Z1 epifluorescence microscope (Zeiss).

For laser microirradiation, cells grown in 35 mm glass bottom microwell dishes (MatTek) were first pre-sensitized in DMEM medium containing 0.1 μg/mL of Hoechst 33342 for 60 min before replacing it with fresh medium containing 10 μM EdU. After incubating for 20 min, the EdU-containing medium was replaced with phenol red free medium (FluoroBrite, Invitrogen) and cells were irradiated with the 364 nm laser line on a LSM510 confocal microscope (Zeiss) equipped with a heated stage. Cells were allowed to recover for

10-15 min prior to pre-extraction (5 min on ice) and processing for immunofluorescence. ZEN Blue (Zeiss) was used to quantify fluorescence intensities of laser stripes.

DNA fiber assay

Asynchronous MEFs or B cells were labeled with 50 μM CldU for 30min, washed with warm PBS and then sequentially to 250 μM IdU for 30min. After completion of IdU labeling, cells were washed again in warm PBS and incubated with 4mM HU for 3 hours before they were collected and resuspended in cold PBS at a concentration of 0.5×10^6/mL. A volume of 2.5 μL of cell suspension was lysed in 7.5 μL of lysis buffer (200 mM Tris-HCl (pH 7.4), 50 mM EDTA, 0.5% SDS) on glass slides for 8min before DNA fibers were stretched. Fibers were then fixed in cold methanol/glacial acetic acid (ratio 3:1) for 2 minutes, air-dried and left overnight at 4°C. Preparations were rehydrated in PBS and denatured in 2.5 M HCl for 30min, washed with PBS and blocked in PBS containing 2% BSA and 0.2% Tween-20 for 1 hour. Newly replicated DNA tracks were immunostained using anti-BrdU antibodies recognizing CldU (Becton Dickinson, Cat# 347580, 1:100 dilution) and IdU (Abcam, ab6326, 1:100). Secondary antibodies used were goat anti-mouse Alexa Fluor 488 (Molecular Probes, Cat# A11001, 1:200) and anti-rat Cy3 (Jackson ImmunoResearch, Cat# 712-166-153, 1:200). Images were captured at 40X magnification using an Axio Observer Z1 (Zeiss). DNA fiber length was measured using ImageJ software.

Statistics

Statistical significance was calculated using unpaired two-tail t test unless otherwise specified. Chi-square (χ^2) test for goodness of fit was used to compare expected and observed frequencies of live born pups. Mann-Whitney test was used for comparing DNA fiber lengths and PALB2 accumulation along laser-induced stripes. Kaplan-Meier survival analyses (Mantel-Cox test) were used for all survival and tumor studies. All statistical tests were performed in GraphPadPrism except χ^2 tests, which were done in RStudio.